Quantum networks assisted by dark modes in optomagnonic systems

Chengsong Zhao,[1] Zhen Yang,[1] Dawei Wang,[1] Yeting Yan,[1] Chong Li,[1] Zhihai Wang,[2] and Ling Zhou[1,*]
[1]*School of Physics, Dalian University of Technology, Dalian 116024, China*
[2]*Center for Quantum Sciences and School of Physics, Northeast Normal University, Changchun 130024, China*

(Received 20 October 2022; accepted 15 September 2023; published 9 October 2023)

In this paper, we present a scheme to construct a quantum network based on optomagnonic systems where the photon-magnon coupling systems are connected by a waveguide. We derive the effective master equation of magnon modes by eliminating the waveguide modes and optical modes. By diagonalizing the dissipative part of the master equation, we identify dark modes so as to eliminate the effect of the dissipation induced by the waveguide. Employing dark modes, we investigate the quantum state transfer and entangled state generation in the two-node cascaded or chiral quantum network. We extend the method to an N-node quantum network and show the generation of a W state. We also consider the influence of experimental imperfections. Our scheme is meaningful for building a quantum network based on a magnonic system.

DOI: 10.1103/PhysRevA.108.043703

I. INTRODUCTION

Quantum networks are very valuable for many quantum information processes such as quantum computing, communication, and metrology [1–3]. Various schemes for building quantum networks by connecting distant nodes have been proposed [4–10]. The distant nodes, which could be atoms within a cavity [4], superconducting circuits [11], and optomechanical [8] or magnonic systems [12], can be connected through a waveguide, allowing for the distribution of quantum information among these nodes. The ability to achieve high-fidelity quantum state transfer between distant nodes in a quantum network is essential. Toward this goal, a state transfer protocol [4] in a cascaded quantum network has been proposed. Since then, many similar but improved schemes have been developed [5–8,10,13]; e.g., a quantum state transfer protocol independent of the optical properties of the qubit can be achieved by utilizing an optomechanical setting in each node [8], and the quantum state transfer immune to noise can be implemented by introducing an intermediary oscillator [5,7]. Additionally, in a chiral or cascaded quantum network, the generation and transfer of entangled states have also been proposed [14–16]. The related experiments with superconducting circuits [11,17] to transfer a quantum state and to produce an entangled state in quantum networks have been demonstrated.

The magnonic systems, due to their long lifetime and broad tunable frequency range, are an important candidates for building quantum networks [18]. Recently, much progress has been made in hybrid magnonic systems [19–27]. For example, photon-magnon-phonon entanglement [23], the gradient memory [21], the magnon squeezed cat state [28], magnon blockade [29–32], and nonreciprocal transmission [33,34] have been reported, which also demonstrate the excellent ability of the magnon to combine complementary physical systems [24], such as microwave photons [35], superconducting qubits [35], optical photons, and mechanical resonators [36–38]. More importantly, cavity optomagnonics which couples the magnons to the optical photons, similarly to the optomechanical interaction [39], would open up opportunities in optical communication between distant quantum computers [20] and has recently made experimental progress [40] and acquired significant interest such as the microwave-to-optics conversion [41–43], heralded magnon Fock state [44], magnon cat state [45], photon blockade [46], magnon path-entangled states [47], and the Bell test [48]. In Ref. [18], they propose a quantum network based on optomagnonic coupling, where, by pumping the corresponding whispering gallery modes (WGMs), the distant magnon-phonon state transfer and entanglement can be implemented.

In this paper, we propose a scheme for constructing a quantum network with YIG spheres as nodes, using optomagnonic coupling. Employing the quantum network, we investigate the quantum state transfer and entangled state generation. We derive the effective master equations of magnon modes by eliminating the waveguide and optical modes, which allows us to establish the dissipative couplings of magnon modes among different nodes. By diagonalizing the dissipative part of the master equation, we find the dark modes so as to eliminate the effect of dissipation induced by the waveguide. Based on the dark modes, we design the control fields to achieve quantum state transfer and entangled state generations. We show that the deterministic quantum state transfer and entangled state generation in a two-node cascaded or chiral quantum network can be achieved by using the designed control fields. And we also extend this approach to a quantum network of N nodes and show the generation of a W state in three- and five-node quantum networks. Finally, we discuss imperfections in experiments, e.g., the intrinsic dissipation. In order to achieve the high-fidelity quantum state transfer and entangled state generation, a small intrinsic decay rate is

*zhlhxn@dlut.edu.cn

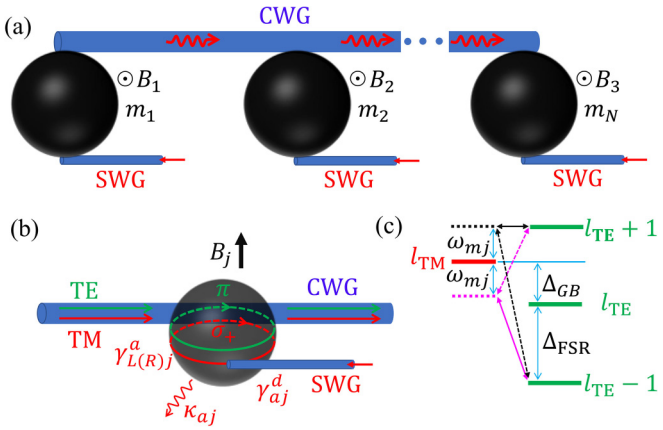

FIG. 1. (a) Schematic of the quantum network consisting of YIG spheres and a common waveguide (CWG). Each YIG sphere is in a bias magnetic field B_j and a coherent driving for the transverse magnetic (TM) mode is introduced by a separate waveguide (SWG). (b) Schematic of the single node. The red (green) arrow indicates TM [transverse electric (TE)] mode. (c) Spectrum of WGMs. The magenta and black dotted horizontal lines denote the frequency of the scattered light. The solid (dotted) double-arrow lines represent the detuning between the scattered light and the WGMs specified by selection rules for clockwise (counterclockwise) input.

required. Hence our scheme offers theoretical support for the construction of quantum networks based on magnonics.

II. THE MODEL AND THE HAMILTONIAN

We consider an N-node quantum network shown in Fig. 1(a), which contains N yttrium iron garnet (YIG) spheres and a common waveguide (CWG). In this quantum network, a node is represented by a YIG sphere in an external uniform magnetic field along the z axis. Each YIG sphere is coupled to a separate waveguide (SWG) so as to introduce a time-dependent coherent pumping.

The detailed configuration of optical modes and the magnon mode in a single node is shown in Fig. 1(b). The magnon modes are sourced from collective spins in the YIG sphere, and in this paper we only consider the Kittel mode. The YIG spheres also support the WGMs which are optical modes confined to the equatorial surface by the total internal reflection [40]. The incident photons, e.g., the transverse magnetic (TM) mode from waveguides, will excite the WGMs in YIG spheres and then the WGMs may be scattered by magnons into other optical modes, e.g., the transverse electric (TE) mode. Due to the zero orbital angular momentum of the Kittel mode, the direction of the scattered photon is the same as that of the incident photon [49].

Additionally, the scattering exhibits nonreciprocal behavior [40,50–52]. Here we consider two orthogonal polarization optical modes: TE and TM modes. The orbital angular moments of TE and TM modes with a given azimuthal mode $l_{\rm TE}$ and $l_{\rm TM}$ are $l_{\rm TE}$ $(-l_{\rm TE})$ and $l_{\rm TM}\mp 1$ $(-l_{\rm TM}\mp 1)$ for counterclockwise (CCW) [clockwise (CW)] circulations, respectively. According to Ref. [50], the resonant frequency difference between TM and TE WGMs of the same azimuthal mode is $\Delta_{\rm GB}\approx 32$ GHz due to the geometric birefringence, and the free spectral range is $\Delta_{\rm FSR}\approx 40$ GHz. The magnon frequency ω_{mj} is tuned to coincide with $\Delta_{\rm FSR}-\Delta_{\rm GB}$. Therefore, due to the angular momentum conservation, for the CW TM mode input, the selection rule of the Stokes scattering process is $l_{\rm TE}=l_{\rm TM}-1$; then the scattered light is far detuned from light specified by the selection rule by $\Delta_{\rm FSR}+\Delta_{\rm GB}-\omega_{mj}$ [magenta solid double arrow in Fig. 1(c)]. However, in the anti-Stokes scattering process with the selection rule $l_{\rm TE}=l_{\rm TM}+1$, the incident TM light excites the σ_+-polarized WGM and then is scattered into the TE mode light with π polarization by the magnon mode [Fig. 1(b)] which is on-resonant with the selection-rule-allowed light [the black solid double arrow in Fig. 1(c)] [50]. Straightforwardly, we can obtain that for the CCW TM mode input, the light of both Stokes and anti-Stokes is far detuned by $\Delta_{\rm FSR}\pm\Delta_{\rm GB}+\omega_{mj}$ [see Fig. 1(c)]. The case of TE mode input can be seen in Ref. [53]. The above nonreciprocal behavior can be summarized as follows: for CCW input, there is no effective interaction, while for CW input, the interaction is $a_jc_j^\dagger m+{\rm H.c.}$, where a_j, c_j, and m_j are the annihilation operators of the TM, TE, and Kittel modes [40]. After implementing a strong coherent driving for the TM mode in each node via SWG with the method shown in Figs. 1(a) and 1(b), the Hamiltonian of the jth node reads

$$H_j=\omega_{aj}a_j^\dagger a_j+\omega_{cj}c_j^\dagger c_j+\omega_{mj}m_j^\dagger m_j+\left(g_ja_jc_j^\dagger m_j+\sqrt{\gamma^d_{aj}}\varepsilon_j^*a_je^{i\omega_{dj}t}+{\rm H.c.}\right),\tag{1}$$

where ω_{aj} (ω_{cj}, ω_{mj}) is the frequency for a_j (c_j, m_j), g_j is the optomagnonic coupling strength, and ε_j represents the coherent driving with the frequency ω_{dj} introduced by SWG with a coupling rate γ^d_{aj}. Hereafter, we refer to a_j (c_j) as the optical pump (signal) mode.

By coupling the modes a_j (c_j) to the CWG, the indirect coupling among different nodes can be reached even if they are separated by a long spatial distance, and thus the quantum network is established [Fig. 1(a)]. Assuming an adiabatic coupling between the CWG and YIG spheres, and due to the orthogonal polarizations of a_j and c_j, the optical signal and pump modes interact with photons of different polarizations in the CWG [49]. We consider the case of the optical pump modes coupling to the CWG. In the frame rotating with $\omega_d\sum_j a_j^\dagger a_j$ (assuming $\omega_{dj}=\omega_d$), the Hamiltonians of the waveguide and the interaction between the CWG and a_j are

$$\begin{aligned}H_w^a&=\sum_{D=L,R}\int\omega b_D^{a\dagger}(\omega)b_D^a(\omega)d\omega,\\ H_{\rm int}^a&=i\sum_{D=L,R}\sum_{j=1}^N\int d\omega\sqrt{\frac{\gamma^a_{Dj}}{2\pi}}\left(b_D^{a\dagger}(\omega)a_je^{-i\omega\tau_{Dj}-i\omega_dt}\right.\\&\quad\left.-a_j^\dagger b_D^a(\omega)e^{i\omega\tau_{Dj}+i\omega_dt}\right),\end{aligned}\tag{2}$$

where $b_D^a(\omega)$ $(D=L,R)$ is the annihilation operator for the left- (L) or right-propagating (R) modes in the CWG with the same polarization as the optical pump modes, $\gamma^a_{L(R)j}$ are the corresponding coupling strengths, and $\tau_{Dj}=x_j/v_D$ with the position x_j of the jth node and the left (right) propagation velocity $v_L<0$ ($v_R>0$). By eliminating the waveguide modes in Hamiltonian (2), we can derive the dynamics

equation of a_j (see Appendix A). When we drive a_j from the right-hand side of the SWG, the optical pump modes circulate predominantly clockwise and will travel to the right along the waveguide (see Fig. 1). In addition, due to the nonreciprocal behaviors caused by the selection rule [Fig. 1(c)], the light with reverse direction cannot effectively excite optical signal modes or generate optomagnonic interactions, which cannot build the desired quantum network. Thus we suppose the optical pump modes predominantly interact with the right-propagating mode, i.e., $\gamma^a_{Rj} \gg \gamma^a_{Lj}$.

Including the coupling of a_j to SWG and the intrinsic dissipation of a_j, the dynamics equation for $\langle a_j\rangle$ is

$$\langle \dot{a_j}\rangle = \left(-i\Delta_{aj} - \frac{\gamma_a}{2}\right)\langle a_j\rangle - ig_j\langle c_j m_j^\dagger\rangle - i\sqrt{\gamma^d_{aj}}\varepsilon_{\mathrm{eff},j} \quad (3)$$

with the detuning $\Delta_{aj} = \omega_{aj} - \omega_d$, total decay rate $\gamma_a = \kappa_{aj} + \gamma^d_{aj} + \gamma^a_{Lj} + \gamma^a_{Rj}$, intrinsic decay rate κ_{aj}, and the effective driving for the jth node, $\varepsilon_{\mathrm{eff},j} = \varepsilon_j - \frac{i}{\sqrt{\gamma^d_{aj}}}\sum'_{D,j,k}\sqrt{\gamma^a_{Dj}\gamma^a_{Dk}}\langle a_k\rangle e^{ik_D x_{jk}}$ [6]. $\sum'_{D,j,k}$ is defined to denote the sum over j, k, and D, where $k_D x_{jk} > 0$, e.g., for $D = R$, we have $x_{jk} > 0$. In the strong pump field limit, neglecting the weak optomagnonic interaction term (g_j is of the order of hertz [40,41,54] and much smaller than the contribution of optical pumping) and replacing a_j with the steady-state expectation value $\langle a_j\rangle_{ss} = \frac{i\sqrt{\gamma^d_{aj}}\varepsilon_{\mathrm{eff},j}}{-i\Delta_{aj}-\gamma_a/2}$, the effective Hamiltonian of the jth node in the rotating frame with $\sum_j \omega_d(a_j^\dagger a_j + c_j^\dagger c_j)$ can be rewritten as

$$H'_j = \Delta_{cj}c_j^\dagger c_j + \omega_{mj}m_j^\dagger m_j + G_j c_j^\dagger m_j + G_j^* c_j m_j^\dagger, \quad (4)$$

where $\Delta_{cj} = \omega_{cj} - \omega_d$ and the enhanced effective coupling strength $G_j = g_j\langle a_j\rangle_{ss}$. The effective coupling G_j is proportional to the effective driven field $\varepsilon_{\mathrm{eff},j}$, which allows us to generate a time-dependent effective coupling $G_j(t)$ by slowly adjusting $\varepsilon_{\mathrm{eff},j}(t)$ [6,44]. The time-dependent classical driving is introduced by coupling YIG spheres with SWGs (see Fig. 1). Similar to the optical pump modes, the optical signal modes c_j also couple to the CWG; however, c_j interacts with the photons whose polarization direction is perpendicular to the polarization direction of the optical pumping mode [49]. Although the optical pump modes are dominant in the CWG, the optical signal modes can still be coupled together through the CWG.

The master equation to describe the indirect coupling of modes c_j in different nodes is (see Appendix A)

$$\dot{\rho} = -i[H'_{\mathrm{node}}, \rho] + \sum_D\sum_j \frac{\gamma_{Dj}}{2}\mathcal{D}[c_j^\dagger, c_j](\rho) - \sum'_{D,j,k}\sqrt{\gamma_{Dj}\gamma_{Dk}}(e^{-ik_D x_{jk}}[\rho c_k^\dagger, c_j] + \mathrm{H.c.}), \quad (5)$$

where $H'_{\mathrm{node}} = \sum_j H'_j$, $\mathcal{D}[o_a, o_b](\rho) = 2o_b\rho o_a - o_a o_b\rho - \rho o_a o_b$, and $\gamma_{L(R)j}$ is the coupling rate to the left- and right-propagating modes. The second line in Eq. (5) indicates the dissipative coupling between different nodes. Due to the direction of the driving field ε_j and the nonreciprocal scattering, the optical signal photons are mainly coupled to the right-propagating mode, $\gamma_{Rj} > \gamma_{Lj}$. In the following, we focus on the case of $\gamma_{Rj} \gg \gamma_{Lj}$ corresponding to the cascaded quantum networks. Many proposals for quantum state transfer are also based on a cascaded quantum network [6,8]. In addition, we analyze the case of a chiral quantum network, which is important in chiral quantum optics [16,55,56]. Note that the optical signal modes may also couple to SWG and exhibit intrinsic dissipation, while the magnon modes also undergo relaxation and pure dephasing [57]. Here, we temporarily ignore these additional dissipations and will analyze them in Sec. V.

III. THE REDUCED MASTER EQUATION OF MAGNON MODES

Because the magnon modes have a long lifetime [39], they are a good candidate to work as storage qubits. We focus on transferring a quantum state or generating an entangled state using the magnon modes as storage qubits. To make the dynamical behavior of magnon modes tractable, we assume that the timescale of the optical signal mode c_j reaching its steady state is much shorter than the timescale of the interaction between the optical signal modes and the magnon modes. Thus the optical signal mode c_j can be eliminated and the effective master equation of magnon modes $\mu = \mathrm{tr}_c(\rho)$ can be derived by Nakajima-Zwanzig project operator techniques as

$$\dot{\mu} = -i[H_{\mathrm{eff}}, \mu] + \sum_{jk}\widetilde{S}_{jk}\mathcal{D}[m_j^\dagger, m_k](\mu), \quad (6)$$

with $\widetilde{S}_{jk} = (S_{jk}(\omega_{mk}) + S^*_{kj}(\omega_{mj}))G_j^* G_k/2$. In Eq. (6), we have assumed a vacuum state for the steady state of c_j. For $j = k$, the second term in Eq. (6) denotes the individual dissipation induced by the waveguide; if $j \neq k$, they represent dissipative coupling induced by the waveguide. The effective Hamiltonian of the magnon modes is

$$H_{\mathrm{eff}} = \sum_k\{\omega_{mk} + |G_k|^2\mathrm{Im}[S_{kk}(\omega_{mk})]\}m_k^\dagger m_k - \frac{i}{2}\sum_{j\neq k}[S_{jk}(\omega_{mk})G_j^* G_k m_j^\dagger m_k - \mathrm{H.c.}], \quad (7)$$

describing on-site energy ($j = k$) and the nonlocal interactions between magnon modes ($j \neq k$), similar to Ref. [58]. The detailed deduction of master equation (6) can be seen in Appendix B. We would like to point out that the phase $e^{ik_D x_{jk}}$ due to the distance x_{jk} between different nodes has been considered in the coefficients $S_{jk}(\omega)$.

The dissipative coupling can also support quantum information processing, but its function is not so clear to be understood. By diagonalizing the dissipative part, we can clearly see the effective dissipation channels induced by CWG. We can then design appropriate methods to avoid this dissipation, thus maintaining good quantum coherence. In order to finish that, we introduce the supermodes $m_{dj} = \sum_k U_{jk}m_k$ with the unitary matrix U. Plugging $m_j = \sum_k U^*_{kj}m_{dk}$ into Eq. (6),

$$\dot{\mu} = -i[H_{\mathrm{eff}}, \mu] + \sum_k D_{kk}\mathcal{D}[m_{dk}^\dagger, m_{dk}](\mu), \quad (8)$$

with $D = U\widetilde{S}U^{\dagger}$ [59]. In Eq. (8), we can see that the supermodes m_{dk} couple to the vacuum "reservoirs" with usual form, which represents an effective dissipative channel. In the following, we will illustrate how to use the supermodes to avoid decoherence induced by the CWG.

IV. APPLICATIONS OF THE QUANTUM NETWORK SUPPORTED BY DARK MODES

In this section, we show transferring an arbitrary quantum state and generating entangled states of the magnon modes of different nodes in a quantum network [6,60]. In Sec. IV A, we take a two-node cascaded quantum network as an example to illustrate how to avoid decoherence induced by the CWG by diagonalizing the dissipative part of the master equation. In Sec. IV B, we show the case in a chiral quantum network. Finally, in Sec. IV C, we extend the method to an N-node quantum network. For simplification, in this section, we assume $\omega_{mj} = \Delta_{cj} = \omega_m$, $\gamma_{R_j} = \gamma$, and $\gamma_{L_j} = \gamma_L$.

A. A two-node quantum network with $\gamma_L = 0$

Assuming $k_R x_{21} = 2n\pi$ (n is an integer) and the effective coupling $G_{1(2)}$ as real, we can calculate the coefficients $S_{jj}(\omega_m) = 2/\gamma$ ($j = 1, 2$), $S_{21}(\omega_m) = -4/\gamma$, and $S_{12}(\omega_m) = 0$ (see Appendix C for details).

Then the master equation of the magnon modes of the two-node quantum network can be simplified as

$$\dot{\mu} = -i[H_{\text{eff}}, \mu] + \sum_{j,k=1,2} \widetilde{S}_{jk}\mathcal{D}[m_j^{\dagger}, m_k](\mu), \tag{9}$$

with the effective Hamiltonian in the rotating frame of $\omega_m \sum_{j=1,2} m_j^{\dagger} m_j$,

$$H_{\text{eff}} = \frac{2i}{\gamma} G_1 G_2 (m_2^{\dagger} m_1 - m_1^{\dagger} m_2), \tag{10}$$

and the matrix

$$\widetilde{S} = \frac{2}{\gamma}\begin{pmatrix} G_1^2 & -G_1 G_2 \\ -G_2 G_1 & G_2^2 \end{pmatrix}. \tag{11}$$

Following what has been discussed in the previous section, we diagonalize matrix $\widetilde{S}$. It can be found that $\widetilde{S}$ has the eigenvalues $2(G_1^2 + G_2^2)/\gamma$ and 0, and the corresponding eigenstates are

$$\begin{aligned} b &= -\sin\theta m_1 + \cos\theta m_2, \\ d &= \cos\theta m_1 + \sin\theta m_2, \end{aligned} \tag{12}$$

with $\sin\theta = G_1/\Omega$, $\cos\theta = G_2/\Omega$, and $\Omega = \sqrt{G_1^2 + G_2^2}$. Then master equation (9) can be rewritten in the form of Eq. (8):

$$\dot{\mu} = -i[H_{\text{eff}}, \mu] + \frac{2\Omega^2}{\gamma}\mathcal{D}[b^{\dagger}, b](\mu), \tag{13}$$

where

$$H_{\text{eff}} = \frac{i\Omega^2}{\gamma}\sin 2\theta (b^{\dagger} d - d^{\dagger} b). \tag{14}$$

See Eq. (13). The supermode b couples to an equivalent vacuum reservoir which leads to the dissipation of the system; meanwhile, the supermode d decouples from the vacuum reservoir. We refer to the supermode b as a bright mode and the supermode d as a dark mode [6]. However, due to the effective swap interaction [see Hamiltonian (14)], the dark mode d could be converted into the bright mode b, which will also induce the dissipation for supermode d. Hence, we need to find a way to inhibit the conversion from the dark mode d to the bright mode b. In the following, we would like to design the time-dependent control fields $G_1(t)$ and $G_2(t)$ [equivalently $\Omega(t)$ and $\theta(t)$] to prevent the swap between the bright and dark modes.

We know that the Fock basis of magnon modes m_j is $|n_{m_1}, n_{m_2}\rangle = \frac{1}{\sqrt{n_{m_1}! n_{m_2}!}} m_1^{\dagger n_{m_1}} m_2^{\dagger n_{m_2}} |0_{m_1}, 0_{m_2}\rangle$. For the supermodes b and d, we define $|n_d(t), n_b(t)\rangle = \frac{1}{\sqrt{n_d! n_b!}}[d(t)]^{\dagger n_d}[b(t)]^{\dagger n_b}|0_d, 0_b\rangle$ with $|0_d, 0_b\rangle = |0_{m_1}, 0_{m_2}\rangle$ [29]. Then we assume the initial state of the network is $|\psi(0)\rangle = \sum_{n_d} c_{n_d}(0)|n_d(0), 0_b\rangle$ with $\sum_{n_d} |c_{n_d}(0)|^2 = 1$, which meets $b|\psi(0)\rangle = 0$. If the state during evolution is maintained as $|\psi(t)\rangle = \sum_n c_{n_d}(t)|n_d(t), 0_b\rangle$, the system will only undergo a unitary evolution. That is, the evolution of the state $|\psi(t)\rangle$ satisfies the Schrödinger equation

$$\begin{aligned} i\frac{\partial|\psi(t)\rangle}{\partial t} &= i\sum_{n_d}\dot{c}_{n_d}(t)|n_d(t), 0_b\rangle + i\sum_{n_d} c_{n_d}(t)\frac{\partial|n_d(t), 0_b\rangle}{\partial t} \\ &= H_{\text{eff}}|\psi(t)\rangle, \end{aligned} \tag{15}$$

with $\frac{\partial|n_d(t),0_b\rangle}{\partial t} = \frac{1}{\sqrt{n_d!}}\frac{\partial[d(t)]^{\dagger n_d}}{\partial t}|0_d, 0_b\rangle$. Using relation (12), we have $\dot{d} = \dot{\theta} b$. Considering $d^{\dagger} b|n_d(t), 0_b\rangle = 0$, we obtain

$$i\frac{\partial|n_d(t), 0_b\rangle}{\partial t} = i\dot{\theta}(b^{\dagger} d - d^{\dagger} b)|n_d(t), 0_b\rangle. \tag{16}$$

Then we have

$$i\sum_{n_d}\dot{c}_{n_d}(t)|n_d(t), 0_b\rangle = [H_{\text{eff}} - i\dot{\theta}(b^{\dagger} d - d^{\dagger} b)]|\psi(t)\rangle. \tag{17}$$

Assuming $\dot{c}_{n_d} = 0$, we have

$$\dot{\theta} = \frac{\Omega^2(t)}{\gamma}\sin 2\theta. \tag{18}$$

If the control field $\Omega(t)$ and $\theta(t)$ meet Eq. (18), in the process of evolution, the state of the network will be $|\psi(t)\rangle = \sum_{n_d} c_{n_d}(0)|n_d(t), 0\rangle_d$. In order to solve the differential equation, we first let $x = \cos 2\theta$, and we have

$$\dot{x} + 2\frac{\Omega^2(t)}{\gamma}(1 - x^2) = 0. \tag{19}$$

The trivial solution of the differential equation is $x = 1$. The nontrivial solution is

$$x = \frac{1 - e^{4\eta(t)+y_0}}{1 + e^{4\eta(t)+y_0}}, \tag{20}$$

with $\Gamma(t) = \Omega^2(t)/\gamma$ and $\eta(t) = \int_0^t \Gamma(t')dt'$, where y_0 is related to the initial condition. Finally, we have the control field $G_{1,2}$:

$$\begin{aligned} G_1 &= \pm\Omega\sqrt{(1 - x)/2}, \\ G_2 &= \pm\Omega\sqrt{(1 + x)/2}. \end{aligned} \tag{21}$$

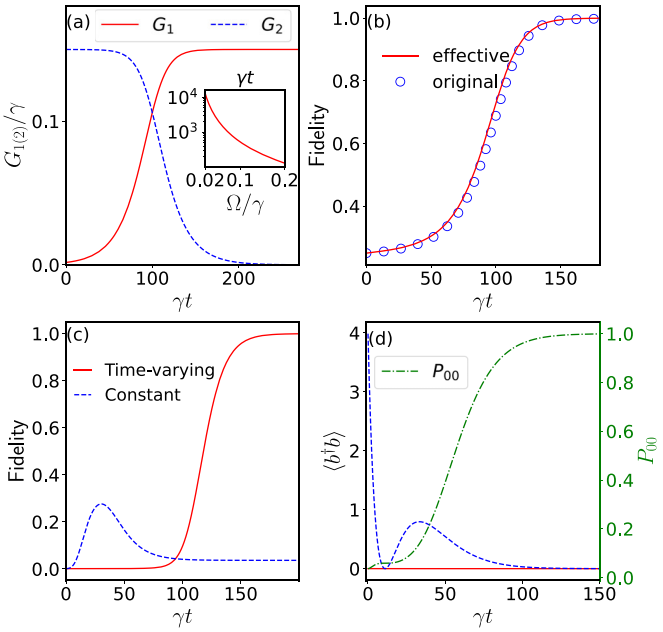

FIG. 2. (a) The designed pulse $G_{1(2)}(t)$. The inset in (a) shows the time to complete a quantum state transfer versus $\widetilde{\Omega}/\gamma$. (b) The evolution of the fidelity, where the red solid line and blue circle correspond to the dynamical evolution governed by Eqs. (5) and (9), respectively. (c) The fidelity of transferring the cat state $|\alpha_+\rangle$ using the time-varying couplings $G_{1(2)}$ in (a) (red solid line) and the constant couplings $G_1 = G_2 = \widetilde{\Omega}$ (dashed blue line). (d) The expectation value $\langle b^\dagger b\rangle$ corresponding to (c), and the probability $P_{00} = \langle 0_{m_1}, 0_{m_2}|\mu|0_{m_1}, 0_{m_2}\rangle$ when $G_{1(2)}(t) = \widetilde{\Omega}$ (the left y coordinate). The parameters are $\widetilde{\Omega} = 0.15\gamma$, $\alpha = 2$, $y_0 = -9$, and $y_{\max} = 10$.

Now we are in the position to illustrate the quantum state transfer by using the control fields (21). We find that $d \to m_1$ when $\theta \to 0$, and $d \to m_2$ when $\theta \to \pi/2$. Based on condition (18), the state of the network is

$$|\psi(t)\rangle = \sum_{n_d} c_{n_d}(0)|(n_d)_{m_1}, 0_{m_2}\rangle(\theta = 0)$$
$$= \sum_{n_d} c_{n_d}(0)|0_{m_1}, (n_d)_{m_2}\rangle(\theta = \pi/2). \quad (22)$$

Hence an arbitrary quantum state of the first node m_1 can be transferred to the second node m_2 if the control field $\theta(t)$ satisfies the conditions $\theta(t = 0) \to 0$ and $\theta(t \to \infty) \to \pi/2$. Because the condition $\theta(t = 0) \to 0$ requires $x(t = 0) = (1 - e^{y_0})/(1 + e^{y_0}) \to 1$, we need to set $y_0 \to -\infty$ (in the actual calculation, y_0 can be set to, for example, -9). The choice of $\Omega(t)$ is not unique and here we set a simple control field; that is, $\Omega(t) = \widetilde{\Omega}$ is time independent. And in order to complete the quantum state transfer ($\theta \to \pi/2$), the condition $4\Gamma t + y_0 = y_{\max} \to \infty$ is required (in simulation, the fidelity can usually be greater than 0.99 when we set $y_{\max} = 10$). Then the total duration to complete the state transfer is $\gamma t = \frac{y_{\max} - y_0}{4(\Omega/\gamma)^2}$, which means as $\widetilde{\Omega}/\gamma$ increases, the time to complete a quantum state transfer decreases dramatically as shown in the inset in Fig. 2(a). Due to the intrinsic dissipation in magnon modes, we expect a shorter duration (see Sec. V), i.e., a larger $\widetilde{\Omega}$. However, $\widetilde{\Omega}/\gamma$ cannot be too large in order to ensure the validity of master equation (6). The exact values for $\widetilde{\Omega}$, and the pulse shapes $G_{1(2)}$ are shown in Fig. 2(a). Now we show the quantum state transfer from the first node to the second node, using the time-dependent functions $G_{1(2)}$ designed in Fig. 2(a), that is, $|\psi\rangle_{m_1} \otimes |0\rangle_{m_2} \to |\psi_{\rm tar}\rangle = |0\rangle_{m_1} \otimes |\psi\rangle_{m_2}$ with arbitrary states $|\psi\rangle_{mj}$. From Eq. (5), after a long enough time evolution, the two optical signal modes are in a vacuum state. Thus for Eqs. (9) and (5), we define the fidelity $F = \langle\psi_{\rm tar}|\rho|\psi_{\rm tar}\rangle$ and $F = \langle 0_{c1}, 0_{c2}|\langle\psi_{\rm tar}|\rho|\psi_{\rm tar}\rangle|0_{c1}, 0_{c2}\rangle$, respectively. In Fig. 2(b), by using Eqs. (9) and (5), we plot the fidelity of transferring a qubit state $|\psi_q\rangle_{m_1} = \rangle 1/\sqrt{2}(|0\rangle_{m_1} + |1\rangle_{m_1})$ with the initial state of the vacuum state $|0_{c_1}, 0_{c_2}\rangle$ in the optical signal mode c_j. As we can observe, the fidelity can reach 1, which illustrates that the pulse shapes obtained above can implement the deterministic quantum state transfer, and the fidelity of Eq. (5) agrees well with that of Eq. (9), which implies the validity of the effective master equation (9). Notably, in Fig. 2(b), we have assumed $k_R x_{21} = 2n\pi$. When $k_R x_{21} \neq 2n\pi$, by the substitution $G_2 \to G_2 e^{ik_R x_{21}}$, the phase in coefficient $S_{21}(\omega_m) = 2e^{ik_R x_{21}}/\gamma$ can be canceled out. Then the matrix $\widetilde{S}$ and the effective Hamiltonian are exactly the same as in the case of $k_R x_{21} = 2n\pi$, for instance, $\widetilde{S}_{21} = \widetilde{S}^*_{12} = -2e^{ik_R x_{21}} G_1[G_2 e^{ik_R x_{21}}]^*/\gamma = -2G_1 G_2/\gamma$. We can generalize this conclusion to an N-node cascaded network; by the substitution of G_j with $G_j e^{ik_R x_{j1}}$, the phase $e^{ik_R x_{jk}}$ in $S_{jk}(\omega_m)$ can also be canceled out. Therefore, for arbitrary phase $e^{ik_R x_{jk}}$, the deterministic quantum state transfer can also be implemented.

The control fields obtained above can be used to transfer not only a two-level state but also the continuous-variable state, e.g., a cat state. As it is shown in Refs. [5,7,61,62], cat states can be employed to reduce errors of quantum state transfer based on quantum error correction codes. In Fig. 2(c) we plot the fidelity for transferring a cat state $|\alpha_+\rangle = 1/A_+(|\alpha\rangle + |-\alpha\rangle)$ using the time-varying coupling $G_{1(2)}(t)$ designed in Fig. 2(a) and the constant couplings $G_1(t) = G_2(t) = \widetilde{\Omega}$, respectively. In Fig. 2(d), we plot the expectation value $\langle b^\dagger b\rangle$ corresponding to Fig. 2(c). As we can observe from Figs. 2(c) and 2(d), with the time-varying couplings, the fidelity reaches 1, while the expectation value $\langle b^\dagger b\rangle$ remains zero, which means no population in bright mode b. Thus the bright mode really is not involved in the process of the state transfer, and the decoherence is avoided; in this way the deterministic quantum state transfer can be implemented. In contrast, with the constant couplings $G_{1(2)}$, there is a population in bright mode b, then the dissipation channel inevitably affects the quantum state transfer, and the corresponding fidelity is finally almost zero, from Fig. 2(c). Meanwhile, from Fig. 2(d) the probability P_{00} of the vacuum state $|0_{m_1}, 0_{m_2}\rangle$ increases gradually and finally to 1. This implies that the state of the magnon modes is eventually a vacuum state, while the optical photon will be released from the right output channel [6,14,63]. Thus, without the right control shapes, the dark mode will also dissipate through the bright mode.

In addition to transferring a quantum state, the entangled state can be generated by designing the coupling $G_{1(2)}$ based on Eq. (18). We set the control field $\theta(t)$ to meet $\theta(t = 0) \to 0$ and $\theta(t \to \infty) \to \pi/4$. If the initial state $|\psi(0)\rangle = |1_{m_1}, 0_{m_2}\rangle$, the final state $|\psi(t \to \infty)\rangle = 1/\sqrt{2}(|1_{m_1}, 0_{m_2}\rangle + |0_{m_1}, 1_{m_2}\rangle)$ will be a Bell state $|\Psi^+\rangle$. As another example, if the initial state of the first node is a cat state $|\alpha_+\rangle$,

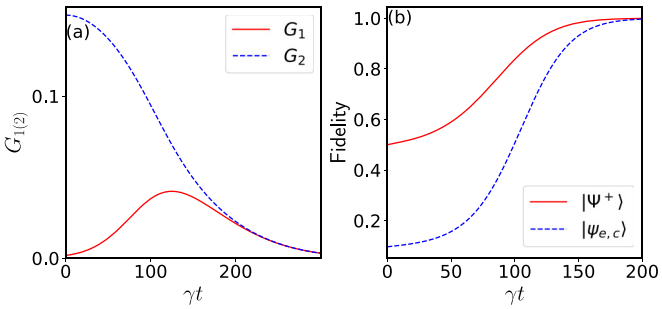

FIG. 3. (a) The pulse shapes of $G_{1(2)}$ of generating entangled states. (b) The evolution of the fidelity for generation of the Bell state $|\Psi^+\rangle$ (red solid line) and entangled cat state $|\psi_{e,c}\rangle$ (blue dashed line). The parameters are the same as in Fig. 2.

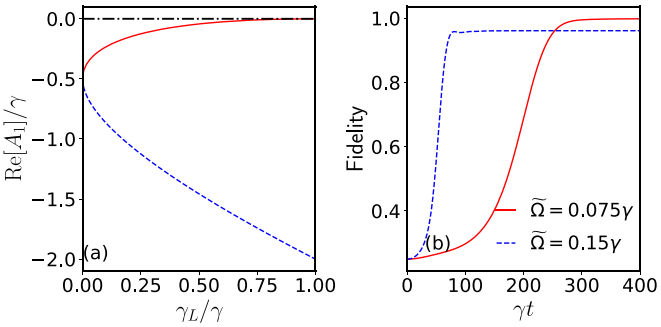

FIG. 4. (a) The real parts of the eigenvalues of the matrix A_1 for $N = 2$ (see Appendix C). (b) The fidelity of transferring the state $|\psi_q\rangle_{m_1}$ by using Eq. (5) with $\widetilde{\Omega} = 0.075\gamma$ (red solid line) and 0.15γ (blue dashed line). In (b), we set $\gamma_L = 0.5\gamma$. The other parameters are the same as in Fig. 2.

the entangled cat state $|\psi_{e,c}\rangle = 1/A_+(|(\frac{\alpha}{\sqrt{2}})_{m_1}, (\frac{\alpha}{\sqrt{2}})_{m_2}\rangle + |(-\frac{\alpha}{\sqrt{2}})_{m_1}, (-\frac{\alpha}{\sqrt{2}})_{m_2}\rangle)$ can be obtained. The control field $\Omega(t)$ satisfying the condition $\theta(t \to \infty) \to \pi/4$ is not unique. Here we set $\Omega(t) = \widetilde{\Omega}e^{-\zeta t^2/2}$ with $\zeta = (\frac{2\widetilde{\Omega}^2\sqrt{\pi}}{-\gamma y_0})^2$. The corresponding pulse shapes $G_{1(2)}(t)$ can be seen in Fig. 3(a). In Fig. 3(b), using master equation (9), we plot the fidelity for generation of a Bell state $|\Psi^+\rangle$ and an entangled cat state $|\psi_{e,c}\rangle$. As one can observe from Fig. 3(b), the fidelity reaching 1 indicates that the Bell state and entangled cat state can be generated.

The generation of the initial cat state in the first node can be seen in Appendix D. Our approach assumes that the magnon mode and superconducting qubit couple simultaneously to a microwave cavity. The odd and even cat states can be obtained by projecting the qubit state to the upper-level and lower-level states, respectively. It is noteworthy that several proposals have been put forward to generate magnon cat states in cavity magnonic systems. For example, the cat states can be obtained via the magnon-photon entanglement described in Ref. [45], a nonlinear radiation-pressure interaction outlined in Ref. [64], and magnon squeezing presented in Ref. [28]. These alternative proposals also can be employed for generating the initial cat state in the first node. In the field of cavity magnonics, the generation of the Bell state has also been explored through dissipative cavity-magnon coupling [65]. However, our proposal distinguishes itself by enabling the generation of the Bell state of distant YIG spheres.

B. A two-node quantum network with $\gamma_L \neq 0$

In this section, we consider a chiral quantum network with $\gamma_L \neq 0$ and $k_D x_{jk} = 2n\pi$ [15]. In this case we still require that the timescale of the magnon-photon interaction is much larger than that of c_j reaching steady state, so that the optical signal modes can be eliminated. However, the timescale of c_j reaching steady state is related with γ_L. We consider the dynamical equation for c_j satisfying $\dot{v}_1 = A_1 v_1$ with $v_1 = [\langle c_1\rangle, \langle c_2\rangle]^T$ (A_1 can be seen in Appendix C). Then the timescale to reach the steady state for mode c_j is related to the maximum real part of the eigenvalues of the drift matrix A_1. In Fig. 4(a), we plot the real parts of the eigenvalues of A_1. We find that with the increase of γ_L/γ, the maximum real part of the eigenvalues (red solid line) gradually increases, which means that the optical signal mode c_j needs more time to reach the steady state. Compared to the case of $\gamma_L = 0$, in order to ensure the validity of Eq. (6), we should reduce the strength of G_j.

The master equation of a two-node chiral quantum network has the same form as Eq. (9) with the effective Hamiltonian

$$H_{\text{eff}} = \frac{2i}{\gamma - \gamma_L} G_1 G_2 (m_2^\dagger m_1 - m_1^\dagger m_2), \tag{23}$$

and $\widetilde{S}_{11(22)} = 2G_{1(2)}^2(\gamma_L + \gamma)/(\gamma - \gamma_L)^2$ and $\widetilde{S}_{21} = \widetilde{S}_{12} = -2G_1G_2(\gamma_L + \gamma)/(\gamma - \gamma_L)^2$ (see Appendix C).

Following similar procedures as in the previous section, we can obtain a differential equation similar to Eq. (18),

$$\dot{\theta} = \frac{\Omega^2}{\gamma - \gamma_L} \sin 2\theta. \tag{24}$$

The difference between Eq. (24) and Eq. (18) is just the substitution $\gamma \to \gamma - \gamma_L$. Hence, similar to Fig. 2(a), by setting $\Omega(t) = \widetilde{\Omega}$, we can obtain the corresponding $G_{1(2)}$ from Eq. (24).

In Fig. 4(b), we plot the fidelity for transferring the state $|\psi_q\rangle_{m_1}$ with the control fields of $\widetilde{\Omega} = 0.075\gamma$ and 0.15γ by using Eq. (5). We find that for the larger $\widetilde{\Omega} = 0.15\gamma$, the fidelity cannot reach 1; in contrast, when $\widetilde{\Omega} = 0.075\gamma$, the fidelity can reach 1. That is consistent with our analysis that a smaller G_j is required to ensure the validity of Eq. (6). Additionally, it should be pointed out that when $k_D x_{jk} \neq 2n\pi$ in the two-node chiral quantum network, the dark mode does not exist, thus the quantum state transfer cannot be achieved. To conclude, in a chiral quantum network, the quantum state transfer can also be achieved similarly to the case of $\gamma_L = 0$.

C. Entangled state generation in an N-node quantum network

Multipartite entangled states play a crucial role in quantum information processing [66,67]. And the ability to entangle multiple nodes in quantum networks is also very essential [1,63]. Here we show how to generate an entangled state in a quantum network containing N nodes by extending the approach above. The master equation of an N-node network

can be simplified as

$$\dot{\mu} = -i[H_{\text{eff}}, \mu] + \sum_{j,k=1}^{N} \widetilde{S}_{jk} \mathcal{D}[m_j^\dagger, m_k](\mu), \tag{25}$$

where $k_R x_{jk} = 2n\pi$ (n is an integer), with the matrix $\widetilde{S}$,

$$\widetilde{S}_{jk} = \frac{2}{\gamma}(-1)^{|j-k|} G_j G_k, \tag{26}$$

and the effective Hamiltonian

$$H_{\text{eff}} = -\frac{2i}{\gamma} \sum_{j>k}^{N} (-1)^{j-k} G_j G_k (m_j^\dagger m_k - \text{H.c.}). \tag{27}$$

Next, we diagonalize the matrix $\widetilde{S}$. We consider that the dimension of $\widetilde{S}$ is $N = 2^M$ for an integer M. The case of $N \neq 2^M$ will be discussed later. To determine the eigenmodes, we begin by defining the auxiliary modes

$$\begin{aligned} b_{1,l_1} &= -\sin\theta_{2^{M-1},l_1} m_{2l_1-1} + \cos\theta_{2^{M-1},l_1} m_{2l_1}, \\ b_{j,l_j} &= \sin\theta_{2^{M-j},l_j} b_{j-1,2l_j-1} + \cos\theta_{2^{M-j},l_j} b_{j-1,2l_j}, \end{aligned} \tag{28}$$

with $j = 2, 3, \ldots, M-1$ and $l_j = 1, 2, \ldots, 2^{M-j}$ (similar to below), and the coefficients $G_{2l_1-1} = \Omega_{2^{M-1},l_1} \sin\theta_{2^{M-1},l_1}$, $G_{2l_1} = \Omega_{2^{M-1},l_1} \cos\theta_{2^{M-1},l_1}$, $\Omega_{2^{M-n+1},2l_n-1} = \Omega_{2^{M-n},l_n} \sin\theta_{2^{M-n},l_n}$, $\Omega_{2^{M-n+1},2l_n} = \Omega_{2^{M-n},l_n} \cos\theta_{2^{M-n},l_n}$ with $n = 2, 3, \ldots, M$. Then the dark modes corresponding to the degenerate eigenvalue of 0 in matrix $\widetilde{S}$ are given by

$$\begin{aligned} d_{1,l_1} &= \cos\theta_{2^{M-1},l_1} m_{2l_1-1} + \sin\theta_{2^{M-1},l_1} m_{2l_1}, \\ d_{k,l_k} &= \cos\theta_{2^{M-k},l_k} b_{k-1,2l_k-1} - \sin\theta_{2^{M-k},l_k} b_{k-1,2l_k}, \end{aligned} \tag{29}$$

with $k = 2, 3, \ldots, M$. The bright mode corresponding to a nondegenerate eigenvalue of $\frac{2\Omega_{1,1}^2}{\gamma}$ in matrix $\widetilde{S}$ is

$$b_{M,1} = \sin\theta_{1,1} b_{M-1,1} + \cos\theta_{1,1} b_{M-1,2}. \tag{30}$$

For the case $N \neq 2^M$, the eigenvalues and eigenmodes can be obtained by setting the corresponding $G_j = 0$ ($j = N+1, N+2, \ldots$). For instance, in order to obtain the eigenvalues and eigenmodes for the case of $N = 3$, we first set $M = 2$. Then by setting $G_4 = 0$ (equivalently $\theta_{2,2} = \pi/2$), the corresponding eigenmodes can be obtained:

$$\begin{aligned} d_{1,1} &= \cos\theta_{2,1} m_1 + \sin\theta_{2,1} m_2, \\ d_{2,1} &= \cos\theta_{1,1}(-\sin\theta_{2,1} m_1 + \cos\theta_{2,1} m_2) + \sin\theta_{1,1} m_3, \\ b_{2,1} &= \sin\theta_{1,1}(-\sin\theta_{2,1} m_1 + \cos\theta_{2,1} m_2) - \cos\theta_{1,1} m_3, \end{aligned} \tag{31}$$

with $G_1 = \Omega_{2,1}\sin\theta_{2,1}$, $G_2 = \Omega_{2,1}\cos\theta_{2,1}$, $G_3 = \Omega_{1,1}\cos\theta_{1,1}$, and $\Omega_{2,1} = \Omega_{1,1}\sin\theta_{1,1}$. And the effective Hamiltonian in the basis of the supermodes is

$$\begin{aligned} H_{\text{eff}} = \frac{i\Omega_{1,1}^2}{\gamma} \{ &-\sin 2\theta_{1,1}(b_{2,1}^\dagger d_{2,1} - b_{2,1} d_{2,1}^\dagger) \\ &+ \sin^2\theta_{1,1} \sin 2\theta_{2,1} [\cos\theta_{1,1}(d_{2,1}^\dagger d_{1,1} - d_{1,1}^\dagger d_{2,1}) \\ &+ \sin\theta_{1,1}(b_{2,1}^\dagger d_{1,1} - d_{1,1}^\dagger b_{2,1})] \}. \end{aligned} \tag{32}$$

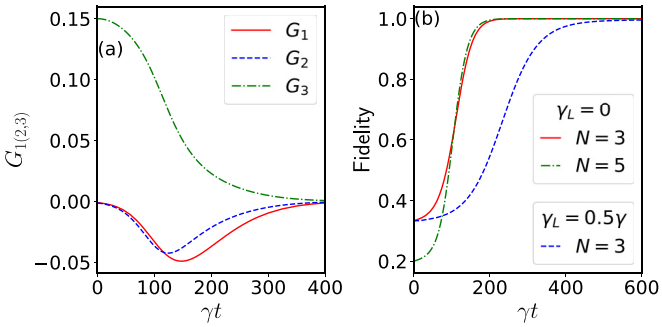

FIG. 5. (a) The pulse shapes of $G_{1(2,3)}$ for generating the W state of $N = 3$ with $\gamma_L = 0$. (b) The evolution of the fidelity of generating the W state for $N = 3$ (red solid line) and $N = 5$ (green dash-dotted line) in a cascaded quantum network. And the blue dashed line shows the fidelity for the case of generating the W state for $\gamma_L = 0.5\gamma$ and $N = 3$ with $\widetilde{\Omega} = 0.075\gamma$. The other parameters are the same as in Fig. 2.

Following the same procedures as in the previous section, the control fields $\theta_{1,1}$ and $\theta_{2,1}$ should satisfy

$$\begin{aligned} \dot{\theta}_{1,1} &= \frac{\Omega_{1,1}^2}{\gamma} \sin 2\theta_{1,1}, \\ \dot{\theta}_{2,1} &= \frac{\Omega_{1,1}^2}{\gamma} \sin^2\theta_{1,1} \sin 2\theta_{2,1}. \end{aligned} \tag{33}$$

We write $x_1 = \cos 2\theta_{1,1}$ and $x_2 = \cos 2\theta_{2,1}$; then the nontrivial solution of the differential equations is ($j = 1, 2$)

$$x_j = \frac{1 - e^{4\eta_j(t) + y_{0j}}}{1 + e^{4\eta_j(t) + y_{0j}}}, \tag{34}$$

with $\eta_j(t) = \int_0^t \Gamma_j(t')dt'$, $\Gamma_1(t) = \Omega_{1,1}^2(t)/\gamma$, and $\Gamma_2(t) = \Omega_{1,1}^2(t)\sin^2\theta_{1,1}(t)/\gamma$.

Next we would like to generate a W state by designing the control fields $G_{1(2,3)}$ from Eq. (33). We assume the initial state $|\psi(0)\rangle = |1_{m_1}, 0_{m_2}, 0_{m_3}\rangle$. And due to $m_1 = \cos\theta_{2,1} d_{1,1} - \sin\theta_{2,1}(\cos\theta_{1,1} d_{2,1} + \sin\theta_{1,1} b_{2,1})$, in order to ensure no population in the bright mode $b_{2,1}$, we set $\theta_{1,1}(0) \to 0$. Then at $t \to \infty$, the state is $|\psi(t \to \infty)\rangle = c_{m_1}|1_{m_1}, 0_{m_2}, 0_{m_3}\rangle + c_{m_2}|0_{m_1}, 1_{m_2}, 0_{m_3}\rangle + c_{m_3}|0_{m_1}, 0_{m_2}, 1_{m_3}\rangle$ with $c_{m_1} = c_{2,1}^i c_{2,1}^f + s_{2,1}^i c_{1,1}^f s_{2,1}^f$, $c_{m_2} = c_{2,1}^i s_{2,1}^f - s_{2,1}^i c_{1,1}^f c_{2,1}^f$, and $c_{m_3} = -s_{2,1}^i s_{1,1}^f$, and the coefficients $s_{2,1}^i = \sin[\theta_{2,1}(0)]$, $c_{2,1}^i = \cos[\theta_{2,1}(0)]$, $s_{1,1}^f = \sin[\theta_{1,1}(\infty)]$, $c_{1,1}^f = \cos[\theta_{1,1}(\infty)]$, $s_{2,1}^f = \sin[\theta_{2,1}(\infty)]$, and $c_{2,1}^f = \cos[\theta_{2,1}(\infty)]$. We find that when $\theta_{1,1,(2,1)}(t)$ satisfies $s_{2,1}^i = \sqrt{\frac{2}{5}}$, $c_{2,1}^i = \sqrt{\frac{3}{5}}$, $s_{1,1}^f = -\sqrt{\frac{5}{6}}$, $c_{1,1}^f = \sqrt{\frac{1}{6}}$, $s_{2,1}^f = \frac{2}{\sqrt{5}}$, and $c_{2,1}^f = \sqrt{\frac{1}{5}}$, the W state ($c_{m_1} = c_{m_2} = c_{m_3} = 1/\sqrt{3}$) can be obtained.

We set $\Omega_{1,1}(t) = \widetilde{\Omega} e^{-\zeta t^2/2}$ with $\zeta = (\frac{2\widetilde{\Omega}^2\sqrt{\pi}}{\gamma(\ln^5 - y_0)})^2$ to meet the above conditions. The corresponding effective coupling $G_{1(2,3)}$ can be seen in Fig. 5(a). And in Fig. 5(b), we plot the fidelity of generating the W state for three nodes. The fidelity reaching 1 illustrates that the W state is obtained. In addition, using the control fields designed in Fig. 5(a), when the initial state is $|\psi(t=0)\rangle = |2_{m_1}, 0_{m_2}, 0_{m_3}\rangle$, the final state is, as shown in Ref. [68], a tripartite high-dimensional

entangled state $|\psi(t\to\infty)\rangle = \frac{1}{3\sqrt{2}}(\sqrt{2}|2_{m_1},0_{m_2},0_{m_3}\rangle + \sqrt{2}|0_{m_1},2_{m_2},0_{m_3}\rangle + \sqrt{2}|0_{m_1},0_{m_2},2_{m_3}\rangle + 2\sqrt{3}|D_2^3\rangle)$ with the Dicke state $|D_2^3\rangle = 1/\sqrt{3}(|1_{m_1},1_{m_2},0_{m_3}\rangle + |0_{m_1},1_{m_2},1_{m_3}\rangle + |1_{m_1},0_{m_2},1_{m_3}\rangle)$ [69]. And the Dicke state $|D_2^3\rangle$ can be concentrated by the approach presented in Ref. [63]. The method of generating the three-node W state can easily be extended to more nodes; as an example, in Fig. 5(b) we show the generation of a W state with five nodes (green dash-dotted line), and the differential equations for five nodes can be seen in Appendix E. These demonstrate the ability of the quantum network to generate multinode entanglement.

Next, we show that the W state can also be generated in a chiral three-node quantum network $\gamma_L \neq 0$ and $k_D x_{jk} = 2n\pi$. From Appendix C, we have $\widetilde{S}_{jj} = 2G_j^2/(\gamma+\gamma_L)$ $(j=1,2,3)$, $\widetilde{S}_{12} = \widetilde{S}_{21} = -2G_1G_2/(\gamma+\gamma_L)$, $\widetilde{S}_{13} = \widetilde{S}_{31} = 2G_1G_3/(\gamma+\gamma_L)$, $\widetilde{S}_{23} = \widetilde{S}_{32} = -2G_2G_3/(\gamma+\gamma_L)$, and the effective Hamiltonian $H_{\rm eff} = 2i/(\gamma-\gamma_L)(G_1G_2m_2^\dagger m_1 - G_1G_3m_3^\dagger m_1 + G_2G_3m_3^\dagger m_2 - \text{H.c.})$. By following the same procedure, we can obtain the differential equations for $\theta_{1,1}$ and $\theta_{2,1}$, which is just a substitution $\gamma\to\gamma-\gamma_L$ in Eq. (33). Hence the effective coupling $G_{1(2,3)}$ in this case can be determined in a similar manner as described in the previous paragraph. And in Fig. 5(b), we plot the fidelity of generating the W state in the chiral quantum network by using Eq. (5). The fidelity also can reach 1, which illustrates that the W state can be generated in the chiral quantum network.

V. THE IMPERFECTIONS

In practice in the experiment, there are some imperfections which were not included in the previous discussion. We now focus on two types of imperfections. The first one is frequency mismatch. In the previous discussion, we assumed that the frequencies of magnon modes m_j and the detuning of optical signal modes c_j were the same: $\omega_{mj} = \Delta_{cj} = \omega_m$. However, when these frequencies do not match, the decoherence induced by the waveguide cannot be avoided, because the dark mode may not exist or the conversion between the bright mode and dark mode cannot be prohibited. So the frequency mismatch will reduce the fidelity of quantum state transfer. In addition, the relaxation and pure dephasing for magnon modes [57] and the additional dissipation for optical signal modes due to coupling to the SWG and intrinsic dissipation also can disrupt the dark modes, leading to a decrease in fidelity. After including these dissipations, the following terms need to be added to master equation (5): $\sum_j \frac{\kappa_{cj}}{2}\mathcal{D}[c_j,c_j^\dagger](\rho) + \sum_j \frac{\kappa_{mj}}{2}\{(n_{m,j}^{\rm th}+1)\mathcal{D}[m_j,m_j^\dagger](\rho) + n_{m,j}^{\rm th}\mathcal{D}[m_j^\dagger,m_j](\rho)\} + \sum_j \kappa_{mj}^{\rm ph}\mathcal{D}[n_{mj},n_{mj}](\rho)$, where $n_{mj} = m_j^\dagger m_j$, κ_{cj} is the addition decay rate of optical signal modes, κ_{mj} and $\kappa_{mj}^{\rm ph}$ are the relaxation and pure dephasing rates of the magnon modes, and $n_{m,j}^{\rm th}$ is thermal magnon number. In this section, we focus on a two-node cascaded quantum network and assume that the low-temperature condition leads to $n_{mj}^{\rm th}\approx 0$. Considering the two imperfections and assuming $\kappa_{cj} = \kappa_c$, $\kappa_{mj} = \kappa_m$, $\gamma_{Rj} = \gamma$, and $\kappa_{mj}^{\rm ph} = \kappa_m^{\rm ph}$, the coefficients become $S_{jj}(\omega_{mj}) = \frac{1}{i(\Delta_{cj}-\omega_{mj})+\widetilde{\gamma}/2}$ $(j=1,2)$, $S_{21}(\omega_{m1}) = -\frac{\gamma}{[i(\Delta_{c,1}-\omega_{m1})+\widetilde{\gamma}/2][i(\Delta_{c,2}-\omega_{m1})+\widetilde{\gamma}/2]}$, $S_{12}(\omega_{m2}) = 0$, with $\widetilde{\gamma} = \gamma+\kappa_c$ when $k_R x_{21} = 2n\pi$. The effective master equation of magnon modes is written as

$$\dot{\mu} = -i[H_{\rm eff},\mu] + \sum_{j,k=1,2}\widetilde{S}_{jk}\mathcal{D}[m_j^\dagger,m_k](\mu) + \sum_{j=1,2}\frac{\kappa_m}{2}\mathcal{D}[m_j,m_j^\dagger](\mu) + \kappa_m^{\rm ph}\mathcal{D}[n_{mj},n_{mj}](\mu), \quad (35)$$

where $H_{\rm eff}$ can be calculated by Eq. (7).

In Fig. 6, using Eq. (35), we plot the fidelity of transferring state $|\psi_q\rangle_{m1}$ under the influence of the aforementioned imperfections. Note that Figs. 2 through 5 show the fidelity in the frame rotating with $\omega_m\sum_j m_j^\dagger m_j$; however, in Fig. 6 we plot the fidelity in the original frame, due to the existence of frequency mismatch. As we can observe from Fig. 6(a), fidelity exhibits rapid oscillation, and the maximum fidelity cannot reach 1, due to the frequency mismatch. From Fig. 6(b), we find that as the degree of frequency mismatch $\omega_{m1}-\omega_{m2}$ increases, the fidelity gradually decreases, while the magnitude of ω_{m2}/γ does not affect the fidelity, by comparing the red solid line and green dots. That implies the fidelity is mainly affected by frequency mismatch rather than the magnitude of frequency. Additionally, the fidelity is found to be insensitive to $\Delta_{cj}-\omega_{mj}$. Figures 6(c) and 6(d) illustrate

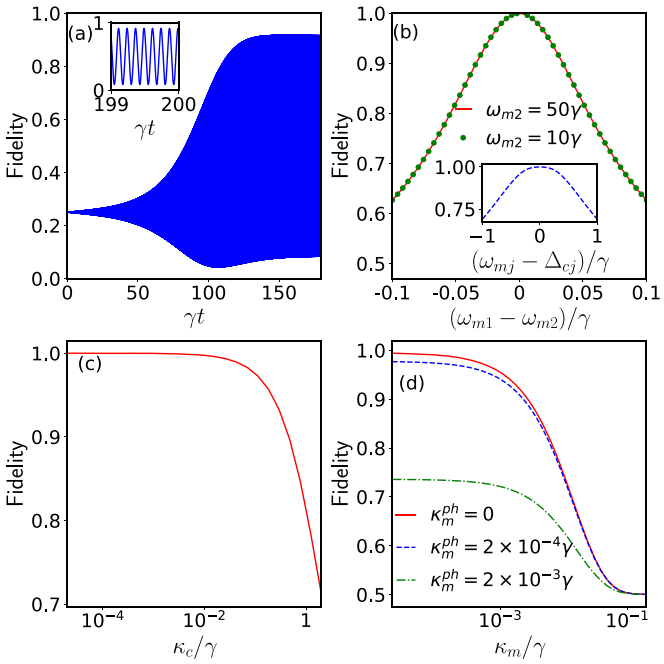

FIG. 6. (a) The evolution of the fidelity with $\omega_{m1}-\omega_{m2} = 0.035\gamma$ and $\Delta_{cj} = \omega_{mj}$. (b) The maximum fidelity versus $\omega_{m1}-\omega_{m2}$ for $\omega_{m2} = 50\gamma$ (red solid line) and 10γ (green dots), when $\Delta_{cj} = \omega_{mj}$. The inset shows the maximum fidelity versus $\Delta_{cj}-\omega_{mj}$ with $\omega_{m1} = \omega_{m2}$. In (a) and (b), we set $\kappa_c = \kappa_m = \kappa_m^{\rm ph} = 0$. (c) The maximum fidelity versus γ_c with $\kappa_m = \kappa_m^{\rm ph} = 0$. (d) The maximum fidelity as functions of κ_m with $\kappa_m^{\rm ph} = 0$ (red solid line), $\kappa_m^{\rm ph} = 2\times10^{-4}\gamma$ (blue dashed line), and $\kappa_m^{\rm ph} = 2\times10^{-3}\gamma$ (green dash-dotted line) when $\kappa_c = 0.02\gamma$. In (c) and (d), we set $\omega_{cj} = \Delta_{cj}$, and $\omega_{m1} = \omega_{m2}$. Except for the green dots in (b), we set $\omega_{m2} = 50\gamma$. The other parameters are the same as in Fig. 2.

that increasing these dissipation rates κ_c, κ_m, and $\kappa_m^{\rm ph}$ leads to a decrease in maximum fidelity. Therefore, achieving high-fidelity quantum state transfer requires small dissipation rates (i.e., $\kappa_c, \kappa_m, \kappa_m^{\rm ph} \ll \gamma$) as well as a small frequency mismatch.

VI. DISCUSSION AND CONCLUSION

A number of researches have been reported to achieve quantum state transfer and entangled state generation by using a time-varying coupling in a cascaded quantum system [4–7,13,63]. In Refs. [4,6], time-dependent control pulses were proposed to transfer a quantum state from one qubit to the next by considering the dark state condition and time-reverse property in the context of quantum trajectories. In Refs. [7,10,13], the conditions and control pulses for transferring a quantum state of oscillators were presented. We would like to highlight that in Ref. [7] the condition for vanishing output fields is equivalent to Eq. (18). In Ref. [63], a protocol for state generation in a multinode cascaded quantum network was proposed. Compared to these proposals, our proposal starting from diagonalizing the dissipative part of the master equation and using the dark modes to avoid the decoherence induced by the CWG not only demonstrates the ability to transfer a quantum state, but also can be easily used to implement the generation of entangled states in a quantum network. Furthermore, our scheme is not limited to two-node quantum networks and can be easily extended to N-node cases. In addition, based on our method, the condition to transfer a quantum state in a chiral quantum network ($\gamma_L \neq 0$) without strictly requiring a cascaded quantum network ($\gamma_L = 0$) can be easily obtained.

Now we discuss how to detect magnon states. Previous experiment [27] has shown that the state of magnons can be measured by measuring the qubit entangled with the magnon. Here we describe a possible method to detect the Bell state of magnon modes in quantum networks. We assume mode m_2 is coupled to an assistant detection qubit with the effective Hamiltonian $H_{\rm de}^{\rm eff} = g_{\rm de} m_2^\dagger m_2 \sigma_z$, which can be achieved by coupling the magnon, qubit, and microwave cavity [27]. We now consider that the detected state of the magnon modes of the two-node quantum network is $c_{10}|10\rangle + c_{01}|01\rangle$ and the qubit is prepared in ground state $|g\rangle$. First, we apply a $\frac{\pi}{2}$ pulse to the qubit ($|g\rangle \rightarrow \frac{1}{\sqrt{2}}(i|e\rangle + |g\rangle)$). Next, we let the qubit interact with m_2 through $H_{\rm de}^{\rm eff}$, and the state becomes $\frac{1}{2}[c_{10}|10\rangle(i|e\rangle + |g\rangle) + c_{01}|01\rangle(ie^{-i\phi_{\rm de}(t)}|e\rangle + e^{i\phi_{\rm de}(t)}|g\rangle)]$ with $\phi_{\rm de} = g_{\rm de} t$. Then, we apply another $\frac{\pi}{2}$ pulse to the qubit, and the state is

$$\frac{i}{\sqrt{2}}[(c_{10}|10\rangle + c_{01}\cos\phi_{\rm de}|01\rangle)|e\rangle + c_{01}\sin\phi_{\rm de}|01g\rangle]. \quad (36)$$

When we choose $\phi_{\rm de} = n\frac{\pi}{2}$ with an integer n, the final state is $c_{10}|10e\rangle \pm c_{01}|01g\rangle$, where the qubit states and the magnon state are entangled. Finally, we measure the state of the qubit $|e(g)\rangle$ to determine the coefficients $c_{10(01)}$. Similarly, to detect the W state, we assume that m_2 and m_3 couple to two separate qubits. Following a similar procedure as above, the final state is $c_{100}|100ee\rangle + c_{010}|010ge\rangle + c_{001}|001eg\rangle$ by setting proper interaction time. Hence the W state can also be detected by measuring qubit states. The detection of qubits and the dispersive coupling between qubit and magnon mode were demonstrated in Ref. [27]. Additionally, there are other ways to measure the magnon state. For example, in Ref. [26], magnon states are characterized by the Wigner tomography, and the density matrix can also be reconstructed by Wigner tomography. The Wigner tomography can also be used to detect cat states obtained in Sec. IV A. And further research is needed to explore more effective methods for detecting magnon states.

Recently, many experiments with optomagnonic systems have been demonstrated [50,54], especially in the coherent conversion of microwave to optical photons [40–43]. In the experiments involving coupling of magnons and WGMs, the optomagnonic coupling $g_j/2\pi$ is typically on the order of a few hertz, such as 1 Hz in Ref. [51], 5.4 Hz in Ref. [54], and 10.4 Hz in Ref. [40]. By driving the optical pumping modes, for instance, the TM polarization light in the experiment in Ref. [40], the effective coupling G_j is about 73 kHz and is promising to reach the 10 MHz level, while the desired control pulses can be generated by modulating the strength and phase of the driving fields of optical pumping modes. And some improvements such as scaling down the sphere size to reduce the mode volumes [40] can further enhance the optomagnonic coupling; thus it is hoped that effective coupling will meet the requirements of our proposal in the near future. Additionally, in experiments [54], the external coupling $\gamma \approx 400$ MHz with the quality factor is about 10^5, i.e., $\kappa_c > \gamma$, which does not satisfy the requirements of the proposal [Fig. 6(c)]. However, after careful surface treatment in experiment [40], the quality factor can be improved to $Q \approx 10^6$ and thus $\gamma > \kappa_c$ which is clearly close to the requirements of our propose. The additional dissipation can further reduced by, for example, properly polishing and chemically processing the WGM resonator of the YIG spheres [40,54]. In addition, the relaxation rate κ_m of magnon modes in YIG spheres, which is typically on the order of megahertz [18,33,70] and can even be much smaller than 1 MHz in low temperature [21], satisfies the requirements $\kappa_m \ll \gamma$ for quantum state transfer. The pure dephasing $\kappa_m^{\rm ph}$ can also be suppressed at low temperature [57]. Therefore, the quantum network node needs to be kept at a low temperature to achieve a smaller κ_m and $\kappa_m^{\rm ph}$, which leads to higher fidelity.

In this paper, we present a scheme for building a quantum network based on optomagnonic systems and propose a protocol to achieve quantum state transfer and entangled state generation. First we derive the effective master equation of magnon modes by eliminating the waveguide and optical signal modes, which establishes the dissipative coupling among different nodes. Then we diagonalize the dissipative part of the master equation and design the control fields by considering the dark modes. We show that the deterministic quantum state transfer and the generation of the Bell state and entangled cat state can be achieved in a two-node cascaded or chiral quantum network. Meanwhile, we show that a W state can also be generated in three- and five-node quantum networks. Finally, we consider some imperfections in experiments such as frequency mismatch and intrinsic dissipation and find that a small frequency mismatch is important for achieving the high-fidelity quantum state transfer. Therefore, our scheme is meaningful for achieving quantum networks based on magnonics.

ACKNOWLEDGMENTS

This work is supported by National Natural Science Foundation of China (Grants No. 12274053) and National Key Research and Development Program of China (Grant No. 2021YFE0193500).

APPENDIX A: ELIMINATING THE WAVEGUIDE MODES

In this Appendix, we give the dynamics equation to describe optical pump (signal) modes coupling to the CWG [16,71]. From Hamiltonian (2), we have

$$\dot{b}_{D}^{a}(\omega) = -i\omega b_{D}^{a}(\omega) + \sum_{j}\sqrt{\frac{\gamma_{Dj}^{a}}{2\pi}}a_{j}e^{-i\omega\tau_{Dj}-i\omega_{d}t}, \tag{A1}$$

and for any operator a in the system, we have

$$\begin{aligned}\dot{a} =& i[H_{\rm node}, a] - \sum_{D}\sum_{j}\sqrt{\frac{\gamma_{Dj}^{a}}{2\pi}}\int d\omega\big[b_{D}^{a\dagger}[a_{j}, a] \\ &\times e^{-i\omega\tau_{Dj}-i\omega_{d}t} - [a_{j}^{\dagger}, a]b_{D}^{a}e^{i\omega\tau_{Dj}+i\omega_{d}t}\big],\end{aligned} \tag{A2}$$

with $H_{\rm node} = \sum_{j} H_{j}$. Then we have

$$\begin{aligned}\dot{a} =& i[H_{\rm node}, a] - \sum_{D,j}\sqrt{\gamma_{Dj}^{a}}\Bigg\{b_{D,a}^{in\dagger}\left(t - \frac{x_{j}}{v_{D}}\right)[a_{j}, a] \\ &\times e^{-i\kappa_{D}x_{j}} - [a_{j}^{\dagger}, a]b_{D,a}^{in}\left(t - \frac{x_{j}}{v_{D}}\right)e^{ik_{D}x_{j}}\Bigg\} \\ &- \sum_{D,j,k}\sqrt{\gamma_{Dj}^{a}\gamma_{Dk}^{a}}\Bigg\{a_{k}^{\dagger}\left(t - \frac{x_{jk}}{v_{D}}\right)[a_{j}, a]e^{-ik_{D}x_{jk}} \\ &- [a_{j}^{\dagger}, a]a_{k}\left(t - \frac{x_{jk}}{v_{D}}\right)e^{ik_{D}x_{jk}}\Bigg\}\theta\left(\frac{x_{jk}}{v_{D}}\right),\end{aligned} \tag{A3}$$

where we define $b_{D,a}^{in}(t) = \frac{1}{\sqrt{2\pi}}\int d\omega e^{-i(\omega-\omega_{d})t}b_{D}^{a}(\omega, 0)$, $x_{jk} = x_{j} - x_{k}$, $\tau_{D,jk} = \tau_{D,j} - \tau_{D,k}$, $k_{D} = \omega_{d}/v_{D}$, and $\theta(z)$ via $\theta(z) = 1$ for $z > 0$, $\theta(z) = 1/2$ for $z = 0$, and $\theta(z) = 0$ for $z < 0$. In Eq. (A3), the retardation effect can be neglected when the timescale of the system evolution is much larger than that of the photon propagation in the waveguide, i.e., $|\tau_{D,jk}| \ll \{1/\gamma_{Dj}, 1/G_{j}\}$. That is to say, we can make the following approximation: $a_{j}(t - \frac{x_{jk}}{v_{D}}) \approx a_{j}(t)$ [16].

Similarly, the Heisenberg-Langevin equation of c_{j} coupling to the CWG can be determined, and we will not go into detail. By using $\mathrm{tr}_{c}(\dot{a}\rho) = \mathrm{tr}_{c}(a\dot{\rho})$ and assuming the bath is in a vacuum initially, the master equation form can be obtained [see Eq. (5)].

APPENDIX B: THE REDUCED MASTER EQUATION OF MAGNON MODES

In this Appendix, we employ Nakajima-Zwanzig project operator techniques to derive the master equation of magnon modes. From Eq. (5), the nonunitary dynamical evolution of the system can be rewritten as

$$\dot{\rho} = L\rho, \tag{B1}$$

with the Liouville operator $L = L_{c} + L_{m} + L_{i}$, where

$$\begin{aligned}L_{c}\rho =& -i\left[\sum_{j}\Delta_{cj}c_{j}^{\dagger}c_{j}, \rho\right] + \sum_{D}\sum_{j}\frac{\gamma_{Dj}}{2}\mathcal{D}[c_{j}^{\dagger}, c_{j}](\rho) \\ &- \sum_{D,j,k}{}'\sqrt{\gamma_{Dj}\gamma_{Dk}}(e^{-ik_{D}x_{jk}}[\rho c_{k}^{\dagger}, c_{j}] + \mathrm{H.c.}), \\ L_{m}\rho =& -i\left[\sum_{j}\omega_{mj}m_{j}^{\dagger}m_{j}, \rho\right], \\ L_{i}\rho =& -i\left[\sum_{j}G_{j}c_{j}^{\dagger}m_{j} + G_{j}^{*}c_{j}m_{j}^{\dagger}, \rho\right].\end{aligned} \tag{B2}$$

The projection operator $\mathcal{P}$ takes action on the density matrix, leading to $\mathcal{P}\rho = \mathrm{tr}_{c}(\rho)\otimes\rho_{c}$, where tr_{c} is the partial trace of the optical signal modes, and ρ_{c} is the steady-state density matrix of the optical signal modes. The operator $\mathcal{P}$ and the complementary operator $\mathcal{Q} = 1 - \mathcal{P}$ have the properties $\mathcal{P}^{2} = \mathcal{P}$, $\mathcal{Q}^{2} = \mathcal{Q}$, $\mathcal{P}\mathcal{Q} = \mathcal{Q}\mathcal{P} = 0$. To derive a simple reduced density matrix equation, we need the following relationships:

$$\begin{aligned}\mathcal{P}L_{c} &= L_{c}\mathcal{P} = 0, \\ \mathcal{P}L_{m} &= L_{m}\mathcal{P}, \\ \mathcal{P}L_{i}\mathcal{P} &= 0.\end{aligned} \tag{B3}$$

The first relation results from the trace-preserving Liouville operator $\mathrm{tr}_{c}(L_{c}\rho_{c}) = 0$, and the steady state of the optical signal modes $L_{c}\rho_{c} = 0$. The second relation is true because the projection operator has no effect on the space of the magnon modes. The third is based on the assumption that the first-order moments for the steady state of the optical signal modes are zeros; it is obviously valid if the optical signal modes are in vacuum states. We start from the equations

$$\begin{aligned}\mathcal{P}\dot{\rho} &= \mathcal{P}L\mathcal{P}\rho + \mathcal{P}L\mathcal{Q}\rho, \\ \mathcal{Q}\dot{\rho} &= \mathcal{Q}L\mathcal{P}\rho + \mathcal{Q}L\mathcal{Q}\rho.\end{aligned} \tag{B4}$$

Solving the second of Eqs. (B4) and inserting the solution into the first of Eqs. (B4), we have

$$\mathcal{P}\dot{\rho} = \mathcal{P}L_{m}\mathcal{P}\rho + \mathcal{P}L_{i}\int_{t_{0}}^{t}ds\mathcal{G}(t, s)\mathcal{Q}L_{i}\mathcal{P}\rho(s), \tag{B5}$$

where $\mathcal{G}(t, s) = T_{\leftarrow}e^{\int_{s}^{t}\mathcal{Q}L(u)du}$ with the chronological time ordering $T_{\leftarrow}$ and it satisfies $\partial\mathcal{G}(t, s)/\partial t = \mathcal{Q}L\mathcal{G}(t, s)$. In Eq. (B5), we have assumed $\mathcal{Q}\rho(t_{0}) = 0$ owing to a factorizing initial state $\rho(t_{0}) = \mathrm{tr}_{c}(\rho(t_{0}))\otimes\rho_{c}(t_{0})$. The equation can further be simplified by preserving the lowest-order expansion in the perturbation interaction L_{i}, that is, $\mathcal{G}(t, s) \approx T_{\leftarrow}e^{\int_{s}^{t}\mathcal{Q}[L_{c}(u)+L_{m}(u)]du}$. In addition, we note that the coupling G_{i} is time dependent in Sec. IV. However, the timescale of the coupling G_{i} is much slower than the timescale $1/\gamma_{R(L),j}$. Hence the coupling is considered to be time independent, when the integration is performed. For convenience, we use the variable substitution $\tau = t - s$ and let $t_{0} \to -\infty$.

Equation (B5) can be written

$$\mathcal{P}\dot{\rho} = \mathcal{P}L_m\mathcal{P}\rho + \mathcal{P}\int_0^\infty d\tau L_i e^{(L_c+L_m)\tau} L_i(\tau) e^{-L_m\tau}\mathcal{P}\rho(t). \tag{B6}$$

Note that in Eq. (B6), we have applied the Markovian approximation $\mathcal{P}\rho(t-\tau) = e^{-L_m\tau}\mathcal{P}\rho(t)$.

Finally, it is straightforward to derive the master equation of the magnon modes by inserting Eq. (B2) into Eq. (B6) [72],

$$\dot{\mu} = -i\left[\sum_j \omega_{mj} m_j^\dagger m_j, \mu\right] - \sum_{j,k}[S_{jk}(\omega_{mk})G_j^* G_k \times (m_j^\dagger m_k \mu - m_k \mu m_j^\dagger) + \text{H.c.}], \tag{B7}$$

where $\mu = \text{tr}_c(\rho)$ is the density matrix of the magnon modes, and the coefficients are

$$S_{jk}(\omega) = \int_0^\infty \langle c_j(\tau) c_k^\dagger(0)\rangle e^{i\omega\tau} d\tau, \tag{B8}$$

with the two-time correlation function $\langle o_a(\tau) o_b(0)\rangle = \text{tr}_c(o_a e^{L_c\tau} o_b \rho_c)$ [73,74]. In Eq. (B7), we have assumed that the steady state of c_j is a vacuum state. The calculation of the two-time correlation function will be discussed in Appendix C. In Eq. (B7), we have ignored the high-frequency term, e.g., $e^{\pm i(\omega_{mk}+\omega_{mj})}$, because we assume $\omega_{mj} \gg G_j$. And we rewrite master equation (B7) in the form of a Lindblad superoperator, which can be seen in Eq. (6).

APPENDIX C: THE TWO-TIME CORRELATION FUNCTION

In this Appendix, we give the calculation of the coefficients $S_{jk}(\omega)$ [6,75]. From master equation (5), we can derive the equation for $\langle c_j\rangle$,

$$\langle \dot{c_j}\rangle = \left[-i\Delta_{cj} - \frac{\gamma_{Rj}+\gamma_{Lj}}{2}\right]\langle c_j\rangle - {\sum_{D,j,k}}' \sqrt{\gamma_{Dj}\gamma_{Dk}} e^{ik_D x_{jk}}\langle c_k\rangle. \tag{C1}$$

Then Eq. (C1) can be rewritten in a compact form $\dot{v}_1 = A_1 v_1$ with $v_1 = [\langle c_1(t)\rangle, \langle c_2(t)\rangle, \ldots, \langle c_N(t)\rangle]^T$, $[A_1]_{jj} = -i\Delta_{cj} - \frac{\gamma_{Rj}+\gamma_{Lj}}{2}$, $[A_1]_{jk} = -e^{ik_R x_{jk}}\sqrt{\gamma_{Rj}\gamma_{Rk}}$ for $j > k$ and $[A_1]_{jk} = -e^{ik_L x_{jk}}\sqrt{\gamma_{Lj}\gamma_{Lk}}$ for $j < k$. Then by using the quantum regression theorem [76], the coefficients can be derived,

$$S_{jk}(\omega) = \sum_l \left[\frac{1}{-i\omega - A_1}\right]_{jl}\langle c_l c_k^\dagger\rangle_{ss}, \tag{C2}$$

with the steady-state values $\langle c_l c_k^\dagger\rangle_{ss}$.

For a cascaded quantum network ($\gamma_{Lj} = 0$), the matrix A_1 is lower triangular, and the eigenvalues of the matrix A_1 are $-i\Delta_{cj} - \frac{\gamma_{Rj}}{2}$; thus the quantum network is stable, which is an important prerequisite for eliminating the optical signal modes in Sec. III. The optical signal modes will converge to the steady state ρ_c which is a vacuum state here, after a long time of evolution. Therefore, we have $\langle c_l c_k^\dagger\rangle_{ss} = \delta_{lk}$. Then we can obtain $S_{jk}(\omega) = 0$ for $k > j$, $S_{jk}(\omega) = e^{ik_R x_{jk}}\mathcal{W}_k^j(-i\omega)$ for $j \geqslant k$, with $\mathcal{W}_k^j = -\sqrt{\gamma_{Rj}\gamma_{Rk}}\mathcal{M}^j\mathcal{C}_{j-1}\cdots\mathcal{C}_{k+1}\mathcal{M}^k$ ($j > k$), $\mathcal{W}_j^j = \mathcal{M}^j$, $\mathcal{C}_l = 1 - \gamma_{Rl}\mathcal{M}^l$, and $\mathcal{M}^j(s) = 1/[s + i\Delta_{cj} + \gamma_{Rj}/2]$.

Next we give the coefficients $S_{jk}(\omega)$, when $\gamma_{Lj} \neq 0$. For simplification, we assume $\Delta_{cj} = \omega_m$, $k_D x_{jk} = 2n\pi$ (n is an integer), $\gamma_{Lj} = \gamma_L$, and $\gamma_{Rj} = \gamma$. We have, for odd N, $[\frac{1}{-i\omega_m - A_1}]_{jj} = \frac{2}{\gamma+\gamma_L}$, $[\frac{1}{-i\omega_m - A_1}]_{jk} = \frac{(-1)^{k-j+1}4\gamma_L}{\gamma^2-\gamma_L^2}$ ($k > j$), $[\frac{1}{-i\omega_m - A_1}]_{jk} = \frac{(-1)^{j-k}4\gamma}{\gamma^2-\gamma_L^2}$ ($j > k$); and we have, for even N, $[\frac{1}{i\omega_m - A_1}]_{jj} = \frac{2(\gamma+\gamma_L)}{(\gamma-\gamma_L)^2}$, $[\frac{1}{i\omega_m - A_1}]_{jk} = \frac{(-1)^{k-j}4\gamma_L}{(\gamma-\gamma_L)^2}$ ($k > j$), $[\frac{1}{i\omega_m - A_1}]_{jk} = \frac{(-1)^{j-k}4\gamma}{(\gamma-\gamma_L^2)}$ ($j > k$). When $k_R x_{jk} \neq 2n\pi$, $\frac{1}{-i\omega_m - A_1}$ is complicated and is not shown here. For the two- and three-node quantum networks, the real part of the eigenvalues of the matrix A_1 is negative [see Fig. 4(a)]; then the quantum network is stable. And the steady state ρ_c is a vacuum state; then the coefficients $S_{jk}(\omega_m)$ can be obtained. Additionally, we note that when $\gamma_L = \gamma_R$, the real part of the eigenvalues of the matrix A_1 is zero, which means that the uniqueness of the steady state for optical signal modes cannot be ensured; thus, the optical signal modes cannot be eliminated as was done in Appendix B.

APPENDIX D: THE GENERATION OF A CAT STATE

In this Appendix, we illustrate how to generate a cat state by coupling the magnon mode of the first node to an auxiliary microwave cavity field which couples strongly to a superconducting qubit. The Hamiltonian reads

$$H_{\text{ms}} = \omega_{ca} c_a^\dagger c_a + \omega_s \sigma^\dagger\sigma + J(t)(c_a^\dagger + c_a)(\sigma + \sigma^\dagger) + \omega_{m1} m_1^\dagger m_1 + G_{\text{cm}}(c_a + c_a^\dagger)(m_1 + m_1^\dagger), \tag{D1}$$

where c_a is the annihilation operator of the auxiliary microwave cavity with the frequency ω_{ca}, $\sigma = |e\rangle\langle g|$ is the Pauli operator of the qubit with the frequency ω_s, and $|e(g)\rangle$ is the upper level (lower level) of the qubit. The strength of the interaction between the qubit and the cavity is modulated by $J(t) = J(\cos 2\omega_L t + 1/2)$ and the coupling between the cavity and the magnon is characterized by G_{cm}. We consider that the frequency of the microwave cavity is far-off-resonant with both the superconducting qubit and the magnon mode, i.e., $\omega_{ca} \gg \omega_s, \omega_{m1}$, and the frequency of the qubit, the magnon mode, and the driving field is near resonant, $\omega_s \approx \omega_{m1} \approx \omega_L$. We move to a rotating frame with $\omega_L(\sigma^\dagger\sigma + m_1^\dagger m_1)$, then utilizing the effective Hamiltonian $-iH_{\text{ms}}(t)\int H_{\text{ms}}(t)dt$, the cavity mode can be adiabatically eliminated. We assume the microwave cavity is in a vacuum state and neglect the high-frequency terms, then the effective Hamiltonian can be derived:

$$H_{\text{ms}}^{\text{eff}} = \Delta_s \sigma^\dagger\sigma + \Delta_{m1} m_1^\dagger m_1 + g_{\text{ms}}\sigma^x(m_1 + m_1^\dagger), \tag{D2}$$

with $\Delta_s = \Delta_s' + \delta_s$, $\Delta_{m1} = \Delta_{m1}' + \delta_m$, $g_{\text{ms}} = -\frac{JG_{\text{cm}}}{2}(\frac{1}{\omega_a-\omega_L} + \frac{1}{\omega_c+\omega_L})$, $\Delta_{s(m1)}' = \omega_{s(m1)} - \omega_L$, $\delta_s = \frac{J^2}{4}(\frac{1}{\omega_a+3\omega_L} - \frac{1}{\omega_c-3\omega_L})$, and $\delta_m = -G^2(\frac{1}{\omega_c+\omega_L} + \frac{1}{\omega_c-\omega_L})$. The Hamiltonian is a Rabi Hamiltonian of the magnon and qubit, which is different

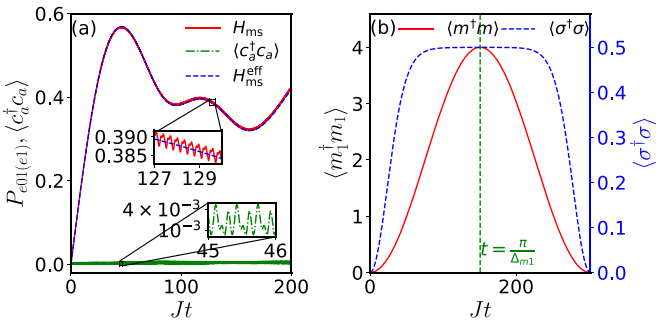

FIG. 7. (a) The evolution of the probability P_{e01} governed by H_{ms} (red solid line) and the probability P_{e1} (blue dashed line) governed by H_{ms}^{eff}. The greed dash-dotted line shows the average photon number $\langle c_a^\dagger c_a\rangle$. Both insets in (a) show the partial enlarged detail. (b) The evolution of the average magnon number $\langle m_1^\dagger m_1\rangle$ (red solid line) and $\langle \sigma^\dagger\sigma\rangle$ (blue dashed line). The parameters are $\omega_{ca}=50J$, $\omega_L=10J$, $G=J$, $\Delta'_{m1}=g_{ms}-\delta_m$, and $\Delta'_s=-\delta_s$.

from the Jaynes-Cummings interaction obtained in experiment [77].

By defining $|\pm\rangle=\frac{1}{\sqrt{2}}(|e\rangle\pm|g\rangle)$, the Hamiltonian (D2) can be rewritten as

$$H_{ms}^{eff}=\Delta_{m1}m_1^\dagger m_1+g_{ms}\tilde{\sigma}^z(m_1+m_1^\dagger), \tag{D3}$$

with $\tilde{\sigma}=|-\rangle\langle+|$, $\tilde{\sigma}^z=|+\rangle\langle+|-|-\rangle\langle-|$. In Eq. (D3), we have assumed $\Delta_s=0$. Utilizing the unitary evolution operator $U_c(t)$ satisfying $i\partial U_c(t)/\partial t=H_{ms}^{eff}U_c(t)$ with the initial state $|g,0_{m_1}\rangle$, the state of the system is

$$\begin{aligned}|\psi_c(t)\rangle&=U_c(t)|g,0_{m_1}\rangle\\&=\frac{1}{\sqrt{2}}e^{i\phi_{ms}(t)}(|+,[\alpha(t)]_{m_1}\rangle-|-,[-\alpha(t)]_{m_1}\rangle)\\&=\frac{1}{2}e^{i\phi_{ms}(t)}(A_-|e,[\alpha_-(t)]_{m_1}\rangle+A_+|g,[\alpha_+(t)]_{m_1}\rangle),\end{aligned} \tag{D4}$$

with $\alpha(t)=-\frac{g_{ms}(e^{i\Delta_{m1}t}-1)}{\Delta_{m1}}$, the odd or even cat states $|\alpha_\pm\rangle=1/A_\pm(|\alpha\rangle\pm|-\alpha\rangle)$, and the normalization constants $A_\pm=\frac{1}{\sqrt{2(1\pm e^{-2|\alpha|^2})}}$. In Eq. (D4), according to the Magnus theory [78], we have used

$$U_c(t)=e^{i\phi_{ms}(t)}e^{g_{ms}\left[\frac{e^{-i\Delta_{m1}t}-1}{\Delta_{m1}}m-\frac{e^{i\Delta_{m1}t}-1}{\Delta_{m1}}m^\dagger\right]\tilde{\sigma}^z}, \tag{D5}$$

with $\phi_{ms}(t)=-\frac{g_{ms}^2}{\Delta_{m1}^2}(\sin\Delta_{m1}t-\Delta_{m1}t)$. From Eq. (D4), one can find that the even or odd cat state can be obtained by projecting the qubit into state $|g\rangle$ or $|e\rangle$, respectively. The state of the system in the original representation can be obtained as $e^{i\omega_L(\sigma^\dagger\sigma+m_1^\dagger m_1)}|\psi_c(t)\rangle$.

In order to check the validity of the approximation from Hamiltonian (D1) to Hamiltonian (D2), we choose $|g,0_{ca},0_{m_1}\rangle$ as the initial state and plot the evolution of the probabilities of $|e,0_{ca},1_{m_1}\rangle$ and $P_{e1}=|\langle e,1_{m_1}|\psi_c(t)\rangle|^2$, as shown in Fig. 7(a). From Fig. 7(a), we see clearly that the results of original Hamiltonian agree very well with that of the effective Hamiltonian; meanwhile, the average photon number is extremely small, $\langle c_a^\dagger c_a\rangle\approx0$, which means that the effective Hamiltonian H_{ms}^{eff} is reliable. In Fig. 7(b), using Hamiltonian (D2), we plot the average magnon number $\langle m_1^\dagger m_1\rangle$ and $\langle\sigma^\dagger\sigma\rangle$. As shown in Fig. 7(b), when $t=\frac{\pi}{\Delta_{m1}}$, the average magnon number reaches its maximum value $|\alpha|^2=4$; meanwhile, $\langle\sigma^\dagger\sigma\rangle$ is $1/2$. So the odd or even cat state with an amplitude $\alpha=2$ can be obtained with a probability of $1/2$. Thus, the desired cat state can be generated in the qubit-photon-magnon system.

APPENDIX E: THE DIFFERENTIAL EQUATIONS FOR FIVE NODES

The differential equations for $\theta_{j,k}$ in a five-node quantum network are

$$\begin{aligned}\dot{\theta}_{1,1}&=\Gamma_5\sin2\theta_{1,1},\\\dot{\theta}_{2,1}&=\Gamma_5\sin\theta_{1,1}\sin2\theta_{2,1},\\\dot{\theta}_{4,1}&=\Gamma_5\sin\theta_{1,1}\sin^2\theta_{2,1}\sin2\theta_{4,1},\\\dot{\theta}_{4,2}&=\Gamma_5\sin\theta_{1,1}\cos^2\theta_{2,1}\sin2\theta_{4,2},\end{aligned} \tag{E1}$$

with $\Gamma_5=\frac{\Omega_{1,1}^2(t)}{\gamma}$.

[1] H. J. Kimble, The quantum internet, Nature (London) **453**, 1023 (2008).

[2] S. Wehner, D. Elkouss, and R. Hanson, Quantum internet: A vision for the road ahead, Science **362**, eaam9288 (2018).

[3] S. Ritter, C. Nölleke, C. Hahn, A. Reiserer, A. Neuzner, M. Uphoff, M. Mücke, E. Figueroa, J. Bochmann, and G. Rempe, An elementary quantum network of single atoms in optical cavities, Nature (London) **484**, 195 (2012).

[4] J. I. Cirac, P. Zoller, H. J. Kimble, and H. Mabuchi, Quantum state transfer and entanglement distribution among distant nodes in a quantum network, Phys. Rev. Lett. **78**, 3221 (1997).

[5] Z.-L. Xiang, M. Zhang, L. Jiang, and P. Rabl, Intracity quantum communication via thermal microwave networks, Phys. Rev. X **7**, 011035 (2017).

[6] K. Stannigel, P. Rabl, A. S. Sørensen, M. D. Lukin, and P. Zoller, Optomechanical transducers for quantum-information processing, Phys. Rev. A **84**, 042341 (2011).

[7] B. Vermersch, P.-O. Guimond, H. Pichler, and P. Zoller, Quantum state transfer via noisy photonic and phononic waveguides, Phys. Rev. Lett. **118**, 133601 (2017).

[8] K. Stannigel, P. Rabl, A. S. Sørensen, P. Zoller, and M. D. Lukin, Optomechanical transducers for long-distance quantum communication, Phys. Rev. Lett. **105**, 220501 (2010).

[9] S. Habraken, K. Stannigel, M. D. Lukin, P. Zoller, and P. Rabl, Continuous mode cooling and phonon routers for phononic quantum networks, New J. Phys. **14**, 115004 (2012).

[10] K. Jahne, B. Yurke, and U. Gavish, High-fidelity transfer of an arbitrary quantum state between harmonic oscillators, Phys. Rev. A **75**, 010301(R) (2007).

[11] C. J. Axline, L. D. Burkhart, W. Pfaff, M. Zhang, K. Chou, P. Campagne-Ibarcq, P. Reinhold, L. Frunzio, S. Girvin, L. Jiang *et al.*, On-demand quantum state transfer and entanglement between remote microwave cavity memories, Nat. Phys. **14**, 705 (2018).

[12] Y.-T. Yan, C. Zhao, Z. Yang, D.-W. Wang, and L. Zhou, Quantum state transfer with cavity–magnonics nodes, J. Phys. B: At. Mol. Opt. Phys. **55**, 195502 (2022).

[13] A. S. Parkins and H. J. Kimble, Quantum state transfer between motion and light, J. Opt. B: Quantum Semiclassical Opt. **1**, 496 (1999).

[14] K. Stannigel, P. Rabl, and P. Zoller, Driven-dissipative preparation of entangled states in cascaded quantum-optical networks, New J. Phys. **14**, 063014 (2012).

[15] W.-K. Mok, D. Aghamalyan, J.-B. You, T. Haug, W. Zhang, C. E. Png, and L.-C. Kwek, Long-distance dissipation-assisted transport of entangled states via a chiral waveguide, Phys. Rev. Res. **2**, 013369 (2020).

[16] H. Pichler, T. Ramos, A. J. Daley, and P. Zoller, Quantum optics of chiral spin networks, Phys. Rev. A **91**, 042116 (2015).

[17] P. Campagne-Ibarcq, E. Zalys-Geller, A. Narla, S. Shankar, P. Reinhold, L. Burkhart, C. Axline, W. Pfaff, L. Frunzio, R. J. Schoelkopf, and M. H. Devoret, Deterministic remote entanglement of superconducting circuits through microwave two-photon transitions, Phys. Rev. Lett. **120**, 200501 (2018).

[18] J. Li, Y.-P. Wang, W.-J. Wu, S.-Y. Zhu, and J. Q. You, Quantum network with magnonic and mechanical nodes, PRX Quantum **2**, 040344 (2021).

[19] H. Yuan, Y. Cao, A. Kamra, R. A. Duine, and P. Yan, Quantum magnonics: When magnon spintronics meets quantum information science, Phys. Rep. **965**, 1 (2022).

[20] B. Zare Rameshti, S. Viola Kusminskiy, J. A. Haigh, K. Usami, D. Lachance-Quirion, Y. Nakamura, C.-M. Hu, H. X. Tang, G. E. Bauer, and Y. M. Blanter, Cavity magnonics, Phys. Rep. **979**, 1 (2022).

[21] X. Zhang, C.-L. Zou, N. Zhu, F. Marquardt, L. Jiang, and H. X. Tang, Magnon dark modes and gradient memory, Nat. Commun. **6**, 8914 (2015).

[22] B. Sarma, T. Busch, and J. Twamley, Cavity magnomechanical storage and retrieval of quantum states, New J. Phys. **23**, 043041 (2021).

[23] J. Li, S.-Y. Zhu, and G. S. Agarwal, Magnon-photon-phonon entanglement in cavity magnomechanics, Phys. Rev. Lett. **121**, 203601 (2018).

[24] D. Lachance-Quirion, Y. Tabuchi, A. Gloppe, K. Usami, and Y. Nakamura, Hybrid quantum systems based on magnonics, Appl. Phys. Express **12**, 070101 (2019).

[25] C. Zhao, Z. Yang, R. Peng, J. Yang, C. Li, and L. Zhou, Dissipative-coupling-induced transparency and high-order sidebands with Kerr nonlinearity in a cavity-magnonics system, Phys. Rev. Appl. **18**, 044074 (2022).

[26] D. Xu, X.-K. Gu, H.-K. Li, Y.-C. Weng, Y.-P. Wang, J. Li, H. Wang, S.-Y. Zhu, and J. Q. You, Quantum control of a single magnon in a macroscopic spin system, Phys. Rev. Lett. **130**, 193603 (2023).

[27] D. Lachance-Quirion, S. P. Wolski, Y. Tabuchi, S. Kono, K. Usami, and Y. Nakamura, Entanglement-based single-shot detection of a single magnon with a superconducting qubit, Science **367**, 425 (2020).

[28] S. Sharma, V. A. S. V. Bittencourt, A. D. Karenowska, and S. V. Kusminskiy, Spin cat states in ferromagnetic insulators, Phys. Rev. B **103**, L100403 (2021).

[29] C. Zhao, X. Li, S. Chao, R. Peng, C. Li, and L. Zhou, Simultaneous blockade of a photon, phonon, and magnon induced by a two-level atom, Phys. Rev. A **101**, 063838 (2020).

[30] F. Wang, C. Gou, J. Xu, and C. Gong, Hybrid magnon-atom entanglement and magnon blockade via quantum interference, Phys. Rev. A **106**, 013705 (2022).

[31] J.-k. Xie, S.-l. Ma, and F.-l. Li, Quantum-interference-enhanced magnon blockade in an yttrium-iron-garnet sphere coupled to superconducting circuits, Phys. Rev. A **101**, 042331 (2020).

[32] Z.-X. Liu, H. Xiong, and Y. Wu, Magnon blockade in a hybrid ferromagnet-superconductor quantum system, Phys. Rev. B **100**, 134421 (2019).

[33] Y.-P. Wang, J. W. Rao, Y. Yang, P.-C. Xu, Y. S. Gui, B. M. Yao, J. Q. You, and C.-M. Hu, Nonreciprocity and unidirectional invisibility in cavity magnonics, Phys. Rev. Lett. **123**, 127202 (2019).

[34] C. Zhao, R. Peng, Z. Yang, S. Chao, C. Li, Z. Wang, and L. Zhou, Nonreciprocal amplification in a cavity magnonics system, Phys. Rev. A **105**, 023709 (2022).

[35] D. Lachance-Quirion, Y. Tabuchi, S. Ishino, A. Noguchi, T. Ishikawa, R. Yamazaki, and Y. Nakamura, Resolving quanta of collective spin excitations in a millimeter-sized ferromagnet, Sci. Adv. **3**, e1603150 (2017).

[36] X. Zhang, C.-L. Zou, L. Jiang, and H. X. Tang, Cavity magnomechanics, Sci. Adv. **2**, e1501286 (2016).

[37] C. A. Potts, E. Varga, V. A. S. V. Bittencourt, S. V. Kusminskiy, and J. P. Davis, Dynamical backaction magnomechanics, Phys. Rev. X **11**, 031053 (2021).

[38] R.-C. Shen, J. Li, Z.-Y. Fan, Y.-P. Wang, and J. Q. You, Mechanical bistability in Kerr-modified cavity magnomechanics, Phys. Rev. Lett. **129**, 123601 (2022).

[39] S. Viola Kusminskiy, H. X. Tang, and F. Marquardt, Coupled spin-light dynamics in cavity optomagnonics, Phys. Rev. A **94**, 033821 (2016).

[40] X. Zhang, N. Zhu, C.-L. Zou, and H. X. Tang, Optomagnonic whispering gallery microresonators, Phys. Rev. Lett. **117**, 123605 (2016).

[41] N. Zhu, X. Zhang, X. Han, C.-L. Zou, C. Zhong, C.-H. Wang, L. Jiang, and H. X. Tang, Waveguide cavity optomagnonics for microwave-to-optics conversion, Optica **7**, 1291 (2020).

[42] J. A. Haigh, R. A. Chakalov, and A. J. Ramsay, Subpicoliter magnetoptical cavities, Phys. Rev. Appl. **14**, 044005 (2020).

[43] R. Hisatomi, A. Osada, Y. Tabuchi, T. Ishikawa, A. Noguchi, R. Yamazaki, K. Usami, and Y. Nakamura, Bidirectional conversion between microwave and light via ferromagnetic magnons, Phys. Rev. B **93**, 174427 (2016).

[44] V. A. S. V. Bittencourt, V. Feulner, and S. V. Kusminskiy, Magnon heralding in cavity optomagnonics, Phys. Rev. A **100**, 013810 (2019).

[45] F.-X. Sun, S.-S. Zheng, Y. Xiao, Q. Gong, Q. He, and K. Xia, Remote generation of magnon Schrödinger cat state via magnon-photon entanglement, Phys. Rev. Lett. **127**, 087203 (2021).

[46] Y.-P. Gao, X.-F. Liu, T.-J. Wang, C. Cao, and C. Wang, Photon excitation and photon-blockade effects in optomagnonic microcavities, Phys. Rev. A **100**, 043831 (2019).

[47] W.-J. Wu, Y.-P. Wang, J.-Z. Wu, J. Li, and J. Q. You, Remote magnon entanglement between two massive ferrimagnetic spheres via cavity optomagnonics, Phys. Rev. A **104**, 023711 (2021).

[48] H. Xie, Z.-G. Shi, L.-W. He, X. Chen, C.-G. Liao, and X.-M. Lin, Proposal for a Bell test in cavity optomagnonics, Phys. Rev. A **105**, 023701 (2022).

[49] S. Sharma, Y. M. Blanter, and G. E. W. Bauer, Light scattering by magnons in whispering gallery mode cavities, Phys. Rev. B **96**, 094412 (2017).

[50] A. Osada, A. Gloppe, R. Hisatomi, A. Noguchi, R. Yamazaki, M. Nomura, Y. Nakamura, and K. Usami, Brillouin light scattering by magnetic quasivortices in cavity optomagnonics, Phys. Rev. Lett. **120**, 133602 (2018).

[51] J. A. Haigh, A. Nunnenkamp, A. J. Ramsay, and A. J. Ferguson, Triple-resonant Brillouin light scattering in magneto-optical cavities, Phys. Rev. Lett. **117**, 133602 (2016).

[52] J. A. Haigh, N. J. Lambert, S. Sharma, Y. M. Blanter, G. E. W. Bauer, and A. J. Ramsay, Selection rules for cavity-enhanced Brillouin light scattering from magnetostatic modes, Phys. Rev. B **97**, 214423 (2018).

[53] A. Osada, A. Gloppe, Y. Nakamura, and K. Usami, Orbital angular momentum conservation in Brillouin light scattering within a ferromagnetic sphere, New J. Phys. **20**, 103018 (2018).

[54] A. Osada, R. Hisatomi, A. Noguchi, Y. Tabuchi, R. Yamazaki, K. Usami, M. Sadgrove, R. Yalla, M. Nomura, and Y. Nakamura, Cavity optomagnonics with spin-orbit coupled photons, Phys. Rev. Lett. **116**, 223601 (2016).

[55] P. Lodahl, S. Mahmoodian, S. Stobbe, A. Rauschenbeutel, P. Schneeweiss, J. Volz, H. Pichler, and P. Zoller, Chiral quantum optics, Nature (London) **541**, 473 (2017).

[56] M. Scheucher, A. Hilico, E. Will, J. Volz, and A. Rauschenbeutel, Quantum optical circulator controlled by a single chirally coupled atom, Science **354**, 1577 (2016).

[57] H. Y. Yuan, W. P. Sterk, A. Kamra, and R. A. Duine, Pure dephasing of magnonic quantum states, Phys. Rev. B **106**, L100403 (2022).

[58] B.-W. Li, Q.-X. Mei, Y.-K. Wu, M.-L. Cai, Y. Wang, L. Yao, Z.-C. Zhou, and L.-M. Duan, Observation of non-Markovian spin dynamics in a Jaynes-Cummings-Hubbard model using a trapped-ion quantum simulator, Phys. Rev. Lett. **129**, 140501 (2022).

[59] T. Ramos, J. J. García-Ripoll, and D. Porras, Topological input-output theory for directional amplification, Phys. Rev. A **103**, 033513 (2021).

[60] D. Awschalom, K. K. Berggren, H. Bernien, S. Bhave, L. D. Carr, P. Davids, S. E. Economou, D. Englund, A. Faraon, M. Fejer, S. Guha, M. V. Gustafsson, E. Hu, L. Jiang, J. Kim, B. Korzh, P. Kumar, P. G. Kwiat, M. Lončar, M. D. Lukin *et al.*, Development of quantum interconnects (quics) for next-generation information technologies, PRX Quantum **2**, 017002 (2021).

[61] M. H. Michael, M. Silveri, R. T. Brierley, V. V. Albert, J. Salmilehto, L. Jiang, and S. M. Girvin, New class of quantum error-correcting codes for a bosonic mode, Phys. Rev. X **6**, 031006 (2016).

[62] L. D. Burkhart, J. D. Teoh, Y. Zhang, C. J. Axline, L. Frunzio, M. H. Devoret, L. Jiang, S. M. Girvin, and R. J. Schoelkopf, Error-detected state transfer and entanglement in a superconducting quantum network, PRX Quantum **2**, 030321 (2021).

[63] H. Ai, Y.-Y. Fang, C.-R. Feng, Z. Peng, and Z.-L. Xiang, Multinode state transfer and nonlocal state preparation via a unidirectional quantum network, Phys. Rev. Appl. **17**, 054021 (2022).

[64] M. Kounalakis, G. E. W. Bauer, and Y. M. Blanter, Analog quantum control of magnonic cat states on a chip by a superconducting qubit, Phys. Rev. Lett. **129**, 037205 (2022).

[65] H. Y. Yuan, P. Yan, S. Zheng, Q. Y. He, K. Xia, and M.-H. Yung, Steady Bell state generation via magnon-photon coupling, Phys. Rev. Lett. **124**, 053602 (2020).

[66] K. Xu, Y.-R. Zhang, Z.-H. Sun, H. Li, P. Song, Z. Xiang, K. Huang, H. Li, Y.-H. Shi, C.-T. Chen, X. Song, D. Zheng, F. Nori, H. Wang, and H. Fan, Metrological characterization of non-Gaussian entangled states of superconducting qubits, Phys. Rev. Lett. **128**, 150501 (2022).

[67] Y. Zhou, B. Li, X.-X. Li, F.-L. Li, and P.-B. Li, Preparing multiparticle entangled states of nitrogen-vacancy centers via adiabatic ground-state transitions, Phys. Rev. A **98**, 052346 (2018).

[68] J.-X. Han, J.-L. Wu, Y. Wang, Y. Xia, Y.-Y. Jiang, and J. Song, Tripartite high-dimensional magnon-photon entanglement in phases with broken $\mathcal{PT}$-symmetry of a non-Hermitian hybrid system, Phys. Rev. B **105**, 064431 (2022).

[69] M. Bergmann and O. Gühne, Entanglement criteria for Dicke states, J. Phys. A: Math. Theor. **46**, 385304 (2013).

[70] Y.-P. Wang, G.-Q. Zhang, D. Zhang, T.-F. Li, C.-M. Hu, and J. Q. You, Bistability of cavity magnon polaritons, Phys. Rev. Lett. **120**, 057202 (2018).

[71] C. W. Gardiner, Driving a quantum system with the output field from another driven quantum system, Phys. Rev. Lett. **70**, 2269 (1993).

[72] Y.-X. Zeng, J. Shen, T. Gebremariam, and C. Li, The study of interference effect in a globally coupled quantum network, Quantum Inf. Process. **18**, 205 (2019).

[73] H. J. Carmichael, *Statistical Methods in Quantum Optics 2: Non-classical Fields* (Springer, Berlin, 2009).

[74] K. Jaehne, K. Hammerer, and M. Wallquist, Ground-state cooling of a nanomechanical resonator via a Cooper-pair box qubit, New J. Phys. **10**, 095019 (2008).

[75] J. H. Lee and H. Seok, Quantum reservoir engineering through quadratic optomechanical interaction in the reversed dissipation regime, Phys. Rev. A **97**, 013805 (2018).

[76] C. Gardiner and P. Zoller, *Quantum Noise: A Handbook of Markovian and Non-Markovian Quantum Stochastic Methods with Applications to Quantum Optics* (Springer, Berlin, 2004).

[77] Y. Tabuchi, S. Ishino, A. Noguchi, T. Ishikawa, R. Yamazaki, K. Usami, and Y. Nakamura, Coherent coupling between a ferromagnetic magnon and a superconducting qubit, Science **349**, 405 (2015).

[78] J.-Q. Liao, J.-F. Huang, and L. Tian, Generation of macroscopic Schrödinger-cat states in qubit-oscillator systems, Phys. Rev. A **93**, 033853 (2016).